Next Nanotechnology 2 (2023) 100019

Contents lists available at ScienceDirect

Next Nanotechnology

journal homepage: www.sciencedirect.com/journal/next-nanotechnology

Review article

Towards the next generation nanorobots

Guoxiang Chen [a,1], Fenyang Zhu [a,1], Alexandra S.J. Gan [a], Brij Mohan [b], Krishna K. Dey [c], Kailiang Xu [d], Gaoshan Huang [a], Jizhai Cui [a], Alexander A. Solovev [a,*], Yongfeng Mei [a,e,f,g,*]

[a] Department of Materials Science & State Key Laboratory of Molecular Engineering of Polymers, Fudan University, Shanghai 200433, PR China
[b] Centro de Quimica Estrutural, Institute of Molecular Sciences, Instituto Superior Tecnico, Universidade de Lisboa, Av. Rovisco Pais, 1049-001 Lisboa, Portugal
[c] Discipline of Physics, Indian Institute of Technology Gandhinagar, Gandhinagar, Gujarat 382355, India
[d] Center for Biomedical Engineering, School of Information Science and Technology, Fudan University, Shanghai 200433, PR China
[e] International Institute of Intelligent Nanorobots and Nanosystems, Fudan University, Shanghai 200433, PR China
[f] Shanghai Frontiers Science Research Base of Intelligent Optoelectronics and Perception, Fudan University, Shanghai 200433, PR China
[g] Yiwu Research Institute of Fudan University, Yiwu 322000, Zhejiang, PR China

ARTICLE INFO

Keywords:
Nanorobots
Nanomotors
Motion control
Autonomous propulsion
Microfluidics
Bioapplications

ABSTRACT

Nanorobots with advanced capabilities that can accomplish various tasks have been the focus of significant research interests. Nanorobots can self-propel in different trajectories, be guided using external fields, and interact with objects and the environment. In recent years, various fabrication techniques, such as physical, chemical, microfluidic, and self-assembly methods, have been employed to integrate specific functions. Microfluidic platforms are utilized to encapsulate individual reactions and reaction networks, providing an experimental testbed system for designing the next generation of nanorobots. Due to significant progress in the field, man-made nanobots have been applied for a wide variety of operations. Today, a convergence between biomedical nanoparticles and nanorobots is apparent. This review discusses the next generation of nanorobots, the range of their fabrication techniques, and introduces integrated functions for bio-applications.

1. Introduction

Intelligent nano/micro- motors, active particles, and robots hold tremendous potential to perform demanding tasks and integration into on-chip applications [1]. Due to their extended capabilities to operate in different environments and achieve required biocompatibility nanorobots (NBs) have generated widespread interests [2,3]. In recent years, different NBs' designs have been considered, such as helical structures, surface walkers, cilia, scaffolds, and biohybrids [4]. Chemical propulsion mechanisms have been reported, such as using self-electrophoresis, self-diffusiophoresis, and microbubble recoil [5]. While chemical, surface acoustic forces, and hierarchical materials have been optimized [6,7], other alternative fuels have been developed, such as using carbon dioxide gas to power autonomous motion [8]. NBs generate motive forces on the order of pico- to nanoN, convert chemical to mechanical energy at efficiencies on the order of 10^{-10}, achieve ultrafast speeds up to 350 body lengths per second (bL s^{-1}), and can move in more complex trajectories [9]. NBs can be designed for specific biomedical applications, such as the delivery of cells [10,11], minimally-invasive surgery [12], "on the fly" biosensing in motion [13], and isolation of pathogens [14]. Slippery nano-propellers have been used to penetrate the vitreous body of the eye without damage [15]. Spermbots have shown promising results in ovarian cancer treatment [16].

The fabrication methods of NBs with standard geometries include electrochemical deposition [17], physical vapor deposition [18], rolled-up technology [19], layer-by-layer (LbL) assembly [20], and biohybrid methods [21–23]. Micromotors fabricated using standard methods often lack required biocompatibility [24,25]. A lack of biocompatibility and biodegradability of conventional NBs made of solid-state materials restricted their implementations for in vivo scenarios and therefore impeded further bio-applications [26]. Microfluidics represents a promising platform for controlled encapsulation and release of different materials using monodispersed micro-drops and capsules. For example, enzyme-powered vesicles [27], hydrogel

* Corresponding author.
* Corresponding author at: Department of Materials Science & State Key Laboratory of Molecular Engineering of Polymers, Fudan University, Shanghai 200433, PR China.
E-mail addresses: solovevlab@gmail.com (A.A. Solovev), yfm@fudan.edu.cn (Y. Mei).
[1] These authors contributed equally

https://doi.org/10.1016/j.nxnano.2023.100019
Received 18 May 2023; Received in revised form 13 September 2023; Accepted 19 September 2023
Available online 29 September 2023

microcapsules with catalytic core [28] have been demonstrated. The integration of microfluidics and nanozymes materials systems with NBs has recently proposed a new direction [29]. Nanoparticle-shelled bubble-microbots with high buoyancy and self-assembly behaviors have been fabricated using glass capillary microfluidics [30]. Liu et al. developed a microfluidic electrospray technique to fabricate porous microparticles with high biocompatibility for three-dimensional cell culture [31]. Hybrid hydrogel capsules also showed several advantages, including high stability and monodispersity, allowing for three-dimensional culture and the generation of human islet organoids from induced pluripotent stem cells [32]. Feng's group presented a Janus Mg-based magnetic NBs for ultrasound imaging and navigation [33]. Yu et al. employed a microfluidic spinning method to fabricate helical NBs for tissue repair by embedding biocompatible hydrogels into cell-seeding microcarriers [34].

Versatile methods to control the motion of NBs have been developed, such as using external fields (e.g., electrical, optical, magnetic, light and ultrasound), by changing fuel concentration, composition, chemical gradients, and light sources [35–37]. Directional control of autonomous nanosystems using a magnetic field was developed to guide the motion of NBs without affecting their speeds [38]. Various magnetic shapes, such as magnetized wormlike mesoporous silica nanotubes with attached $CoFe_2O_4$ nanoparticles, have been tested. Subsequently, the cargo was released using an alternating magnetic field (0.5 mT, 100 Hz) [39]. Specific programmable trajectories of NBs using motion control in bio-systems have been addressed using advanced soft computing techniques [40]. Particular attention attracted optical resonance or light-driven NBs using the generation of a motive force by the angular momentum exchange between the NBs and photons [41]. Versatile NBs' control methods using modulation of light propagation, polarization, frequency, and intensity lead to control of local photocatalytic and photo-electrochemical reactions [42,43]. Automated motion control is complicated to achieve using conventional methods. Recently, the application of an Artificial Intelligence (AI) planner, vision feedback control, to determine optimal control and three-dimensional paths using helical-propelled NBs, led to new interesting directions of precise motion control of NBs towards advanced applications [44]. In addition, AI integration in amalgamation with a neural network system can advance real-time biomedical tasks [45].

The field of NBs progress in the direction of advanced nano/-micromachines with specific functions. For instance, programmable DNA-based NBs have been used for autonomous tasks such as motion, sensing, and actuation, leading to the demonstration of nanotools for precision medicine [46]. It is believed that self-catalyzing chemical reactions and non-equilibrium synthetic nanomaterials with functions similar to living matter, such as adaptation, self-healing, and self-replication, are achievable in the near future. A nonlinear chemical system is one of the examples of non-living systems that mimic some biological properties. For example, the Belousov-Zhabotinsky reaction is a redox reaction catalyzed by a metal ion. It reproduces several characteristics observed in living systems, for example, periodic oscillations, patterns formation, hysteresis, and bifurcations. Therefore, self-propelled objects powered or coupled to nonlinear chemical reactions is a promising research direction that can lead to the discovery of biomimetic principles.

NBs for bio-applications can be divided into several categories, including minimally-invasive surgery, cell/molecules delivery, isolation of pathogens, cancer isolation, and diagnostics tools. For instance, recently shown NBs and biohybrids [47] have been proposed for targeted disease treatments, such as cardiovascular, cancer, gastrointestinal, orthopedic, and ophthalmic [48,49]. However, specific safety issues have been considered, including safe motion, biocompatibility, and biodegradability [50,51]. More importantly, the convergence of NBs and classical nanoparticle/drug delivery fields are observed. In this scenario, all previous knowledge and expertise in toxicity study and therapeutic delivery of nanomaterials can be translated to NBs-driven biomedical advances.

This review paper discusses the next generation of NBs with advanced fabrication methods, specific functions, and bio-applications. Fig. 1**(a)** illustrates classical materials systems of NBs, such as nanorods, tubes, spheres, and helixes. To achieve advanced functionalities, e.g., on-the-fly virus sensing [52], and chemically powered synthetic living systems, it is envisioned that NBs connection with information technology is required [53]. Fig. 1**(b)** shows an application of digital microfluidics for encapsulation of functional NBs with coupled sub-systems (CS: catalytic sub-system, AS: automotive sub-system, IS: information sub-system). Advantages of microfluidics consist in encapsulation of virtually any material to screen conditions and achieve required coupling among cycles, reaction networks, information storage, information processing systems, feedback loops, and chemo-mechanical responses. The focus of this review lies in the intersection of nanomotors or nanorobots with microfluidics and reaction networks, a subject matter not comprehensively addressed in prior research. While numerous studies have explored nanomotors, nanorobots, and microfluidics individually, the gap concerning their integration with reaction networks is filled by this manuscript. The significance of this combination and its potential applications in various fields such as targeted drug delivery, environmental monitoring, and advanced manufacturing processes are elucidated. To emphasize the contributions of our review, a comparative analysis with prior work is provided, highlighting aspects not previously covered. This interdisciplinary approach opens up new directions for innovative applications and more complex micromachines.

2. Multiple fabrication techniques for micro/nanorobots

To date, a great number of advanced fabrication methods have been applied to fabricate classical NBs, including electrochemical deposition, physical vapor deposition, strain engineering nano/-microtubes, and direct laser writing [54,55]. However, the rapid demand of bio-compatibility and accurate manipulation has resulted in developing the microfluidic for the synthesis of micro/nanorobots. It manipulates

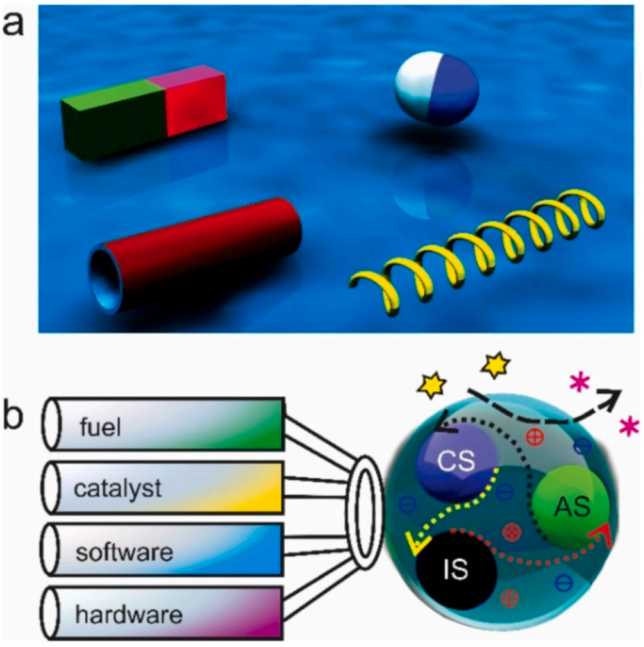

Fig. 1. Scheme proposes next generation of NBs with integrative functions. (a) Schematic image of standard solid state-based nano- rod, tube, sphere, and helical structures. (b) Envisioned microfluidic method for integration of subsystems to achieve intelligent NBs (CS: catalytic sub-system, AS: autonomous sub-system, IS: information sub-system).

small amounts of fluids in microscale channel to form a desired device. Compared with conventional fabrication methods, it offers many merits, such as bio-compatibility, complex integration, and desired chemical composition.

Recently, many works are reported for the fabrication of NBs using microfluidics. For instance, Zhang et al. used a capillary glass device with an off-chip photopolymerization strategy to induce droplet templates for the preparation of NBs using three-phase immiscible flows (silicone oil-hydrophilic poly (ethylene glycol) diacrylate (PEGDA)-lipophilic 1, 6-Hexanediol diacrylate (HDDA)), shown in Fig. 2(a). The immiscible property between the PEGDA and HDDA, an off-chip photopolymerization strategy can improve production efficiency by decreasing the blocking of the microdevice. For instance, altering the different phases' flow rates allows control over droplet templates' size and composition. The porous PEDGA structure also increases the contact area between the functional nanoparticles and the surrounding media, including Ag, TiO_2, and Fe_3O_4 [56]. In addition, Chen et al. developed glass capillary microfluidics to prepare self-propelled Janus NBs, shown in Fig. 2(b). Subsequently, the speed of the micromotors was improved, and well-defined fabrication parameters were achieved [57]. Besides, Feng et al. demonstrated a one-step microfluidic preparation process for multiphase Janus NBs consisting of PLGA, HCG lipid, and p (BMA-co-DAMA-co-MMA), which revealed the generation of triple-phase particles using phase separation method [58].

The electrochemical template-assisted method is a facile, low-cost strategy for fabricating advanced NBs. Fig. 2(c, d) depicts template-based electrosynthesis of helical nano swimmers [59,60]. Liu et al. used an electrochemical method for the fabrication of MnO_2 tubular micromotors, shown in Fig. 2(c). Initially, 5 μm diameter polycarbonate template is prepared with an Au layer sputtered on one side (as a working electrode) and PEDOT as outer layers are deposited. Subsequently, electrodeposition of MnO_2 on the inner layers is used, followed by the dissolution of the template in methylene chloride solution to release the NBs. In addition, the relationship between the physicochemical properties of NBs and catalytic performance under different electrodeposition modes has been investigated. Results revealed that changing electrodeposition parameters could tailor the NBs' catalytic performance [59]. Li et al. described the templates-based electrosynthesis method of helical nano swimmer-based NB, shown in Fig. 2(d). In the shown example, atomic layer deposition is used to deposit Al_2O_3 layers on the porous polycarbonate template, followed by the sputtering of a thin Au layer on one side of the porous film as a working electrode and deposition of Pd/Cu layers on the porous membrane. The Pd nanorods are obtained upon the removal of Cu and templates [60].

Combination of fluidic, assembly, and physical methods have been used to prepare NBs. For example, Adams et al. applied glass capillary microfluidics to inject toluene with silica nanoparticles between the inner and outer capillaries. In addition, the air stream was injected through the inner capillary. Subsequently, the functionalization is used using an e-beam depositing Ti/Pt layers on the dry microbubble structures, shown in Fig. 2(e). Nanoparticle-shelled bubbles are self-propelled by converting hydrogen peroxide into oxygen bubbles and water. It was

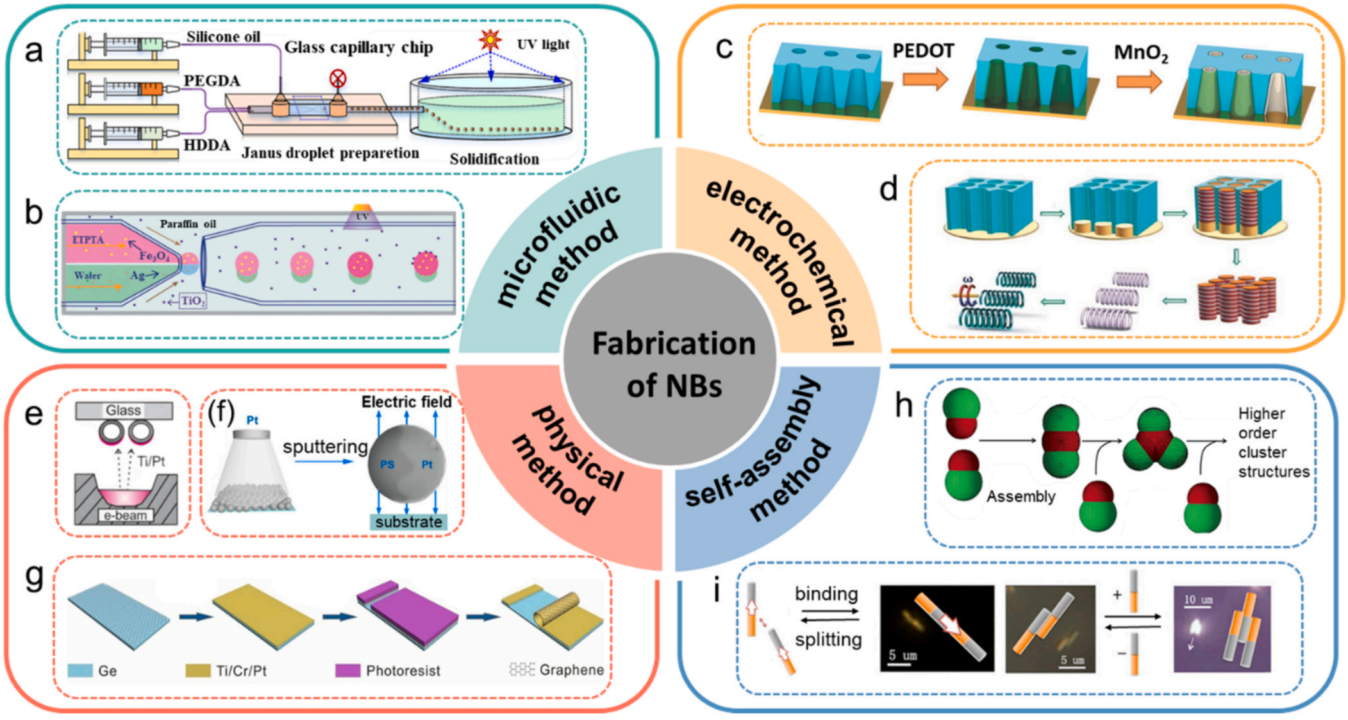

Fig. 2. Fabrication methods of micro/-nanorobots. (a) Schematic of the microfluidic system used for generation of Janus microrobots. (b) The dispersed phase contains two phases: the water phase and the photocurable ETPTA oil phase. Yellow dots denote the ETPTA oil phase containing Fe_3O_4 nanoparticles with a size of 20 nm. The water phase contains modified Ag nanoparticles (50 nm) shown as red dots. The continuous phase is paraffin oil mixed with TiO_2 nanoparticles (20 nm). Span 80 is the surfactant used to vary the interfacial tension between paraffin oil and water. (c) Schematic diagram of template-assisted electrodeposition procedures of PEDOT/MnO_2 micromotors. (d) Schematic illustration of the template-based fabrication of helical magnetic nano swimmers. (e) Schematic image of electron-beam evaporation of Ti/Pt layers on SiO_2 microbubbles in a vacuum. (f) Schematic diagram of Janus micromotors fabricated by ion sputtering. (g) Schematic image of the fabrication process of the rolled-up graphene/Ti/Cr/Pt tubular micromotor. (h) Dynamic self-assembly of electrophoretic nanomotors propelling as a cluster in fuel solutions. (i) 'Hard–soft' particles assembled to colloidal molecules to form higher order cluster structures.
(a) Reproduced with permission [56]. Copyright 2021 Elsevier B.V. (b) Reproduced with permission [57]. Copyright 2017, The Royal Society of Chemistry. (c) Reproduced with permission [59]. Copyright 2018, John Wiley & Sons. (d) Reproduced with permission [60]. Copyright 2014, The Royal Society of Chemistry. (e) Reproduced with permission [30]. Copyright 2020, John Wiley & Sons. (f) Reproduced with permission [61]. Copyright 2022, Elsevier B.V. (g) Reproduced with permission [61]. Copyright 2019, John Wiley & Sons. (h) Reproduced with permission [62]. Copyright 2014, The Royal Society of Chemistry. (i) Reproduced with permission [63]. Copyright 2013, National Academy of Science.

shown how dynamic bubble-bots repel each other, and break free from the microbubble raft, propelling across the air–fuel interface and providing new insights into dynamic self-assembly systems. Besides, gas core structures are widely utilized as contrast agents in biomedical ultrasound-driven imaging of tissue and are of specific use for targeted drug delivery [30]. Meng et al. demonstrated single dispersed polystyrene microspheres fabricated by microfluidics. Fig. 2(f) shows the functionalization process using ion-sputtering, forming self-electrophoretic Janus NBs. The authors also reported dynamic mechanisms influenced by the NB's size, indicating the versatility of microfluidics for the fabrication of NBs [61].

Based on strain engineering, the rolled-up nanotechnology is applied to form the desired tubular shape. Bubble-propelled tubular NBs are demonstrated for the first time in Mei's group [64,65]. Subsequently, the rolled-up nanomembrane method has been widely applied. For instance, Zhang et al. designed catalytic tubular micromotors consisting of graphene doped as the outmost surface and Ti, Cr, and Pt layers deposited on graphene sequentially by e-beam deposition, shown in Fig. 2(g). With graphene's hydrophobic and antibacterial properties, these NBs showed promising results towards in vivo drug delivery and biosensing [19]. Zhao et al. developed a rapid method to produce NBs, which simplified the fabrication of roll-up nanomembranes using magnetron sputtering [66]. Substantial research has been devoted to self-assembly methods. Skelhon et al. reported the NBs fabrication method for self-assembly of Janus microparticles, consisting of "soft" and "hard" spheres. Stirring the solutions causes the collision of Janus particles. The "soft" part serves as an adhesive, thus assembling particles in groups, shown in Fig. 2(h), a new strategy for the self-assembly methods of NBs [62]. Wang et al. reported a study on the self-assembly of Pt/Au nanorods prepared by electrodeposition. When inserted into hydrogen peroxide solution, the nanorods self-propel and assemble due to a self-induced electric field originating from the electrocatalytic oxidation and reduction reactions occurring on the anode and cathode, respectively. Subsequently, nanorods are self-assembled in both the longitudinal and axial directions by the electric field and propelled by the electrophoresis, shown in Fig. 2(i) [63].

Wu et al. introduced a Janus capsule motor fabricated using a layer-by-layer, template-based self-assembly in conjunction with microcontact printing. The Pt nanoparticles on the surface serve to decompose hydrogen peroxide fuel, thus powering the motor's movement [67]. In another work, Wu et al. demonstrated a well-defined polymer multilayer tubular nanomotor. This structure was created via nanoporous template-assisted layer-by-layer assembly and offers a promising avenue for the design of multifunctional nanorockets [68].

The biohybrid nanomotors originated from nature provide a great source of inspiration for the design of artificial motors [69]. Hortelao et al. demonstrated an Enzyme-powered nanomotors through immobilizing urease and gold nanoparticles on the surface of mesoporous silica nanoparticles [70]. The obtained nanomotors displayed higher capability to swim across complex paths inside microfabricated phantoms compared with inactive nanomotors. In addition, Magdanz et al. developed a sperm-flagella driven micro-bio-robot by combining a single sperm cell with a microtube [71]. The incorporation of thin films of magnetic material into the microtube offers the possibility to remotely control the motor under an external magnetic field.

Electrochemical deposition is cost-effective and does not necessitate harsh environments, but is limited in terms of material options and the complexity of the structures it can produce. Physical vapor deposition allows for a broader range of materials and intricate designs, but often at a higher cost and with potential issues in biocompatibility. Rolled-up nanotechnology facilitates mass production and versatile designs but may struggle with quality consistency and bio-compatibility. The self-assembly technique can create highly complex structures through layer-by-layer assembly of components, yet it is time-intensive and demands strict environmental conditions [55]. In light of these factors, microfluidic methods have emerged as particularly promising, offering a balanced combination of rapid prototyping, high bio-compatibility, and precise manipulation capabilities [75,76]. Microfluidics can be used to adjust the geometric characteristics and functions of NBs by incorporating functional nanoparticles and manipulating the fluid flow parameters [61,77]. Moreover, the microfluidic approach is applied, for example, to generate multiple droplets and jets with complex morphologies and configurations. By designing the structure of the microfluidic chips, glass capillaries and changing different phases of fluids, NBs can be fabricated without any template [3,78]. Keller et al. depicted the enzyme-driven gel NBs based on the high-throughput design of asymmetric, biocompatible hydrogel microparticles composed of poly (ethylene glycol) diacrylate(PEGDA) and dextran (Fig. 3(a)), featuring the biocatalyst positioned in the PEDGA phase. The NBs are fabricated using spontaneous phase separation of the microfluidic droplets [72]. In addition, by integrating Pt-coated silica nanoparticles (PSNs) into the microfluidic droplet generating system, Liu and co-workers established a facile droplet microfluidics approach for continuous and direct synthesis of the porous particles [31]. In another example, Zhu et al. utilized glass capillary microfluidics to generate complex water-in-oil-in-water (W/O/W) double emulsion drops and oil-in-water (O/W) emulsion drops followed by their photopolymerization, shown in Fig. 3(b). Three hydrogel NBs fabrication strategies have been explored: i) microcapsules with thin shells, ii) liquid cores with dispersed catalytic Pt nanoparticles, water-cored microcapsules, iii) and homogeneous microparticles selectively coated with Ti/Pt catalytic layers. The disadvantage of the short-range dynamic responses of hydrogels is overcome by the lightweight, lateral capillary forces and self-propelling capabilities of the NBs [28]. Zou's group presented a microfluidic method for the one-step generation of multifunctional NBs. Using a capillary microfluidic system with dual inner injections, shown in Fig. 3(c), composite structured polymer NBs with two distinct cores of Pt-integrated and Fe_3O_4-dispersed hydrogels have been obtained. The Pt-integrated cores eject bubbles when immersed in the hydrogen peroxide solution, while the Fe_3O_4-dispersed cores enable the magnetic guiding of NBs. It shows promising results in biomedical applications such as drug delivery, including effective motion and recyclability of microscale objects [73]. In a related study, Tang et al. reported a facile microfluidic template method to fabricate magnetic hybrid NBs with helical structures. The fabrication procedures of magnetic hybrid NBs are shown in Fig. 3(d). First, synthesized Fe_3O_4-nanoparticles-containing helical Ca-alginate microfibers from microfluidic coiled flows, followed by bio-silicification and controllable dicing to engineer their rigid hollow helical structures. Subsequently, helical structures are engineered in open tubular or closed compartmental volumes by switching bio-silicification sequences and dicing. This work provides a facile and efficient strategy for the controllable fabrication of magnetic hybrid NBs with hollow helical structures for rotation-based locomotion, cargo transport, encapsulation, and delivery [74]. A microfluidic platform integrated with flow lithography for continuously generating helical microparticles has been developed. The mixed liquid flow consists of Na-alginate and poly (ethylene glycol) diacrylate (PEG-DA) injected in the calcium chloride solution in a microchannel, and microfiber with a spiral shape is formed. Subsequently, the fiber is partially exposed to ultraviolet light with a photomask to polymerize the exposed area. Finally, the helical NBs are obtained by the degradation of the unexposed area [79].

To date, the intelligent collective behavior of micro/nanorobots still lack intelligent behaviors to autonomously regulate their distribution and adapt to the environmental change [80]. Recently, Yang et al. designed an autonomous environment-adaptive microrobot swarm navigation enabled by deep learning-based real-time distribution planning [81].11 Based on deep learning, the microrobot swarm were enabled to learn optimal distributions in extensive unstructured environmental morphologies. There would be great space to combine the intelligent algorithms to the nanorobots, improving them to autonomously make appropriate decisions in the uncertain environments.

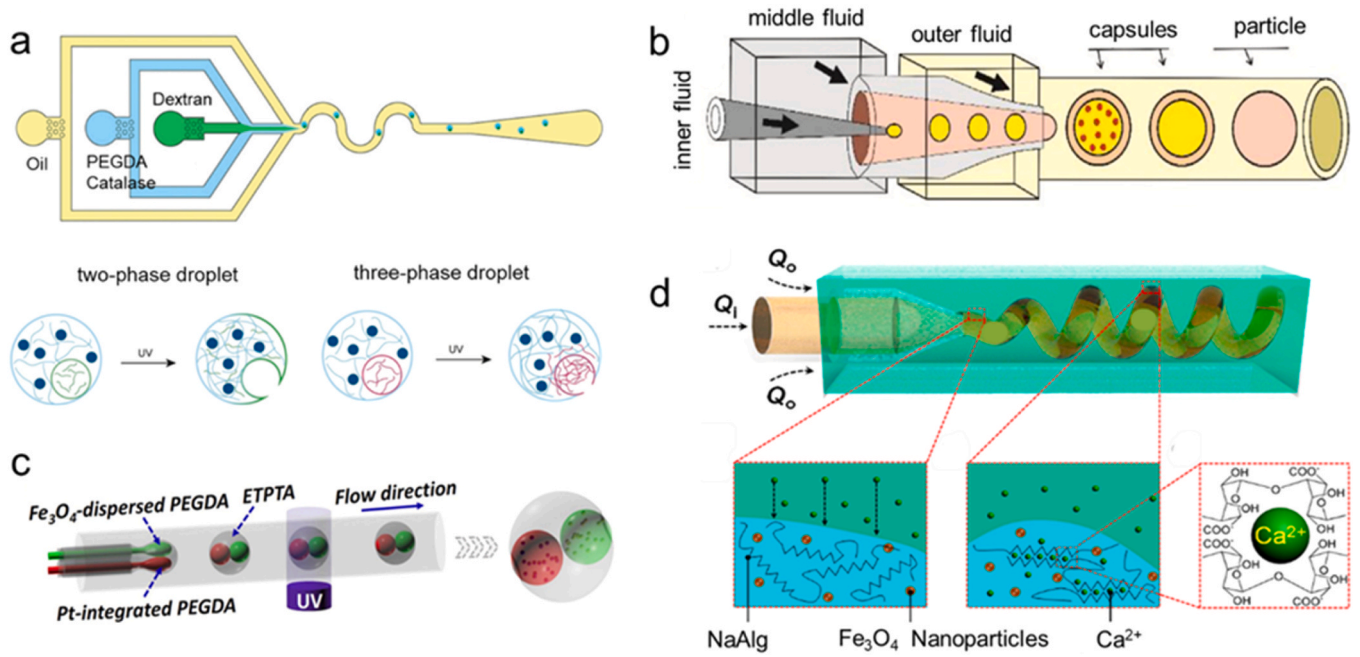

Fig. 3. Microfluidic fabrication methods of micro/nanorobots. (a) A microfluidic chip is used to construct ATPS droplets, three inlets—oil, PEGDA, and dextran—and one outlet. At the first cross junction, an ATPS jet is formed, which is emulsified at the second cross-junction. (b) Schematic of microfluidic glass capillary device used for the generation of hydrogel particles. Capsules from complex emulsion drops and optical microscopy image of double emulsion drop formation in glass capillary microfluidic device. After generation, the double emulsions are irradiated with UV light (not shown) to photo-polymerize the shells of the microcapsules and particles. (c) Micromotor generation by the capillary microfluidic system with dual Inner injections and real-time microscope image of the microfluidic emulsification of the composite double emulsions with various numbers of cores. (d) for synthesizing magnetic helical Ca-Alg microfibers via interfacial cross-linking reactions and between alginate and Ca^{2+}.
(a) Reproduced with permission [72]. Copyright 2018, Wiley, VCH. (b) Reproduced with permission [28]. Copyright 2019, IOP Publishing. (c) Reproduced with permission [73]. Copyright 2018, American Chemical Society. (d) Reproduced with permission [74]. Copyright 2018, American Chemical Society.

3. Smart motion control and intelligent collective behavior of micro/nanorobots

3.1. Designs of collective behavior of micro/nanorobots

Various methods to control the motion of NBs have been achieved including magnetic field, light, ultrasound, electric field, electrochemical potential, and chemotaxis. Fig. 4(a) shows an example of diffusive chemotactic motion of catalase enzyme in the presence of the hydrogen peroxide substrate. Enzymes are placed in the co-flow configuration in the microfluidic channel It was shown that catalase and urease elongate motion trajectories toward higher concentrations of hydrogen peroxide [82]. Fig. 4(b) shows magnetic CNC/Fe_3O_4 nanomotors that can effectively load doxorubicin anticancer drugs using π–π stacking interactions. The magnetic field is a versatile method to propel, locate NBs near targeted cells, and release therapeutic agents (e.g., using infrared light) [83]. Fig. 4(c) shows glucose driven enzyme-based mesoporous Janus SiO_2 @Au core@shell NBs powered by the near-infrared light. The NBs are powered by glucose using glucose oxidase/catalase catalyst. In addition, thermophoretic/photothermal motive force is generated by the illumination of the mesoporous structure of NBs using NIR light [84]. Fig. 4(d) illustrates another approach to control motion using applied electric (*E*-) fields. Novel architectures of electrodes have been used to utilize AC, and DC *E*-fields and achieve accurate delivery of cargo payloads [85]. Fig. 4(e) discusses an example of NBs speed control, including power switched "on" and "off" using electrochemical potential. The potential has been applied using an Au-fiber working electrode placed close to the NBs to control electrochemically reaction products generated at the surface of NBs [86]. Fig. 4(f) demonstrates ultrasound-propelled Au nanowire-based NBs with ovalbumin antigen for vaccine delivery. In contrast to other external fields, ultrasound enables the effective internalization of NBs into the cytoplasm of the antigen-targeting cells. The technology has a high potential to enhance immunity and immunotherapy [87].

Collective behaviors of animals are common in nature, such as ant colonies, fish schools, and bird flocks. Inspired by natural swarms, collective and swarming behaviors of NBs have attracted considerable interest [88]. To date, various strategies have been established to induce the self-organization of dynamic NBs, within which the units can be either self-propelled by chemical reaction or triggered by external fields, such as a magnetic field, light, an acoustic field, and an electrical field [88,89]. What's more, the obtained collective behaviors of NBs have many current and potential applications in environmental remediation and biomedical engineering, due to the advantages of the collective cooperation of nearby individuals and sizeable specific area of agents.

Magnetic field-driven microrobotic swarms provide a sufficient route for the control of robotics. For instance, Xie et al. applied alternating magnetic fields to program hematite colloidal particles in liquid, chain, vortex, ribbon-like microrobotic swarms and enabled further fast and reversible transformations between them, shown in Fig. 5(a) [90]. Dai et al. demonstrated light-controlled artificial NBs based on a Janus TiO_2/Si nano-tree structure [91]. Under ultraviolet illumination, NBs are programmed to perform phototactic swarms when treated with 3-[2-(2-aminoethylamino)-ethylamino]-propyltrimethoxysilane (AEEA) or decorated with Pt NPs showing positive phototaxis and grafted with 2-(4-chlorosulfonylphenyl)ethyltrimethoxysilane (CSPTMS) showing negative phototaxis, shown in Fig. 5(b). Besides, Wu et al. used a simple ion-exchange interaction in a mixture of self-propelled ZnO nanorod and sulfonated polystyrene (PS) microbeads, resulting in a collective behavior on a hierarchical scale [92]. Due to the attractive osmosis, the sulfonated PS microbeads can approach ZnO nanorods and form tightly bonded core-shell clusters, shown in Fig. 5(c). Such adjacent clusters gradually merge into larger clusters. The long-range and inter-cluster attractions align ZnO-sulfonated PS clusters to form a long stripe.

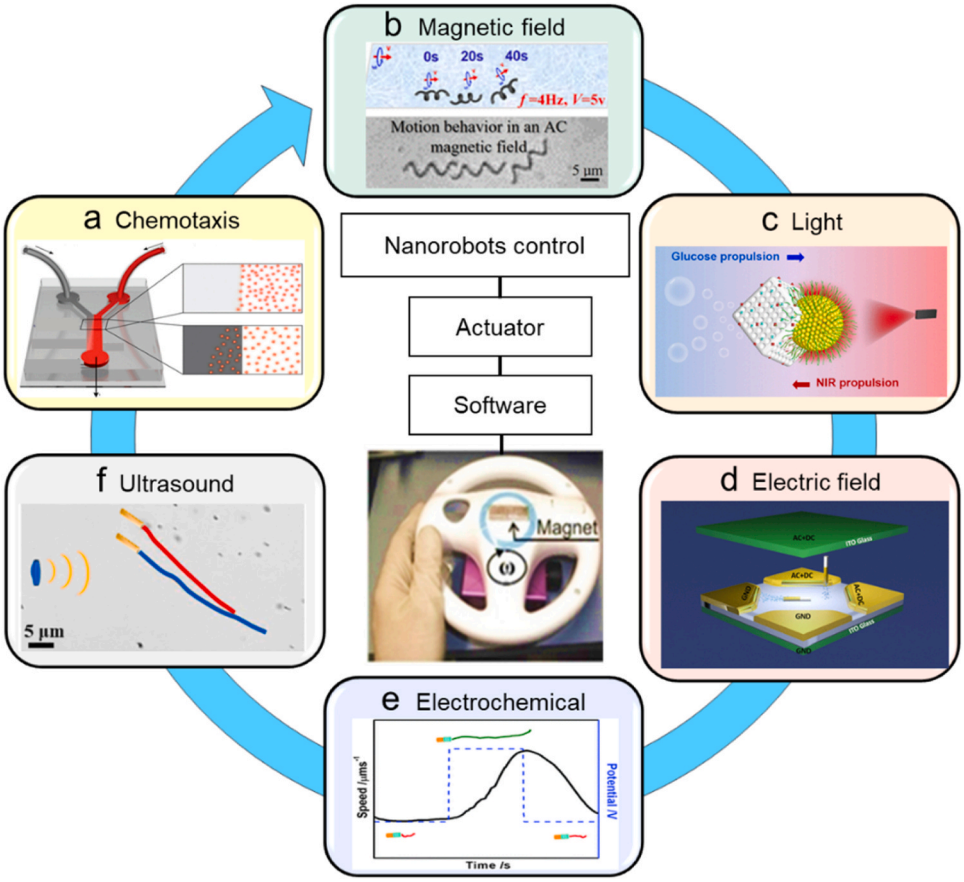

Fig. 4. Concepts of various methods of motion control of NBs. (a) Study of non-biological chemotaxis observed for enzymes in microfluidic channels co-laminar flows.(b) Magnetic field driven helical micromotor structures. (c) Near infrared light-driven propulsion in glucose fuel. (d) Electric field powered nanorod. (e) Modulation of NBs motion using reference electrode immersed in the fluid, i.e., electrochemical potential. (f) Ultrasound-powered method of nanorod-based NBs. (a) Reproduced with permission [82]. Copyright 2013, American Chemical Society. (b) Reproduced with permission [83]. Copyright 2022, American Chemical Society.(c) Reproduced with permission [84]. Copyright 2022, American Chemical Society. (d) Reproduced with permission [85]. Copyright 2018, American Chemical Society. (e) Reproduced with permission [86]. Copyright 2009, The Royal Society of Chemistry.

Moreover, intergroup attraction can lead to further aggregations on a larger scale. Specifically, some sulfonated PS cannot completely exchange the Zn^{2+} released from the ZnO core in some local areas of the deformed clusters, resulting in the repulsive interaction in the large-scale swarm [92].

The acoustic gathering effect is also demonstrated in forming a microswarm of liquid metal agents. Li et al. reported a reconfigurable dynamic assembly based on acoustically actuated eutectic gallium-indium alloy (EGaIn) liquid metal colloidal NBs [93]. It shows various stripes of EGaIn colloidal motors formed at a frequency of 730 kHz. These motor stripes gradually merged into larger striped patterns and self-organized flower-like patterns when the frequency was changed to 722 kHz. The swarm flower-like pattern was dispersed again when the frequency was decreased to 680 kHz, as shown in Fig. 6(a). These EGaIn microswarms can be further manipulated to move by adjusting the frequency of the applied acoustic field. Such collective movements are attributed to the variation of the node planes resulting from the change of frequency of the standing wave acoustic field [93]. Microrobotic swarms responsive to dual stimuli and controlled by hybrid external powers could adapt to more complex environments [94,95]. Recently, combined acoustic power with light illumination was applied to induce the collective behaviors of Janus microrobots, shown in Fig. 6(b) [94]. Driven by the acoustic field, the bowl-like TiO_2/Au microrobot exhibits motion toward its exterior side, caused by the oscillating edges-generated second-order acoustic streaming flow [94]. Therefore, this motion is independent of the position of the TiO_2 and Au layers. Unlike the acoustic-driven motion, the UV light-powered self-prophetic motion is material dependent, which means the NB exhibits motion toward the TiO_2 side. Due to the acoustic pressure gradient, two groups of Janus NBs gather to the low-pressure nodes, with the exterior side facing the pattern's center. After turning on the UV light, the two patterns consisting of Janus NBs with a reversed position of TiO_2 and Au layers show different behaviors: pattern expansion and pattern contraction with the exterior layers of Au and TiO_2, respectively.

Electric field-driven microrobotic swarms provide another route for the control of robotics. In Fig. 6(c), Bricard et al. applied an electric field to insulating particles immersed in a conducting fluid, resulting in the fluctuation of the charge distribution on the particle surface [96]. The formed electrostatic torque caused the particles to rotate randomly, thus showing various collective states. At low area fraction, the rolling particles moved in random directions at the same speed, forming an isotropic gaseous phase. A clear transition to the collective motion was observed by increasing the fraction above a critical value. A macroscopic fraction of the roller self-organizes, and its constituents cruise coherently in the same direction. A homogeneous polar-liquid phase is observed by further increasing the particle fraction, in which the head of the propagating bands catches up with the tail of themselves. These results show that hydrodynamic interactions enable individual particles to perform a directed collective motion [89,96]. Notably, chemically driven active systems at micro- and nanoscales have tremendous potential for biomimetic applications. The recent discovery of molecular chemotaxis has empowered the implementation of targeted active

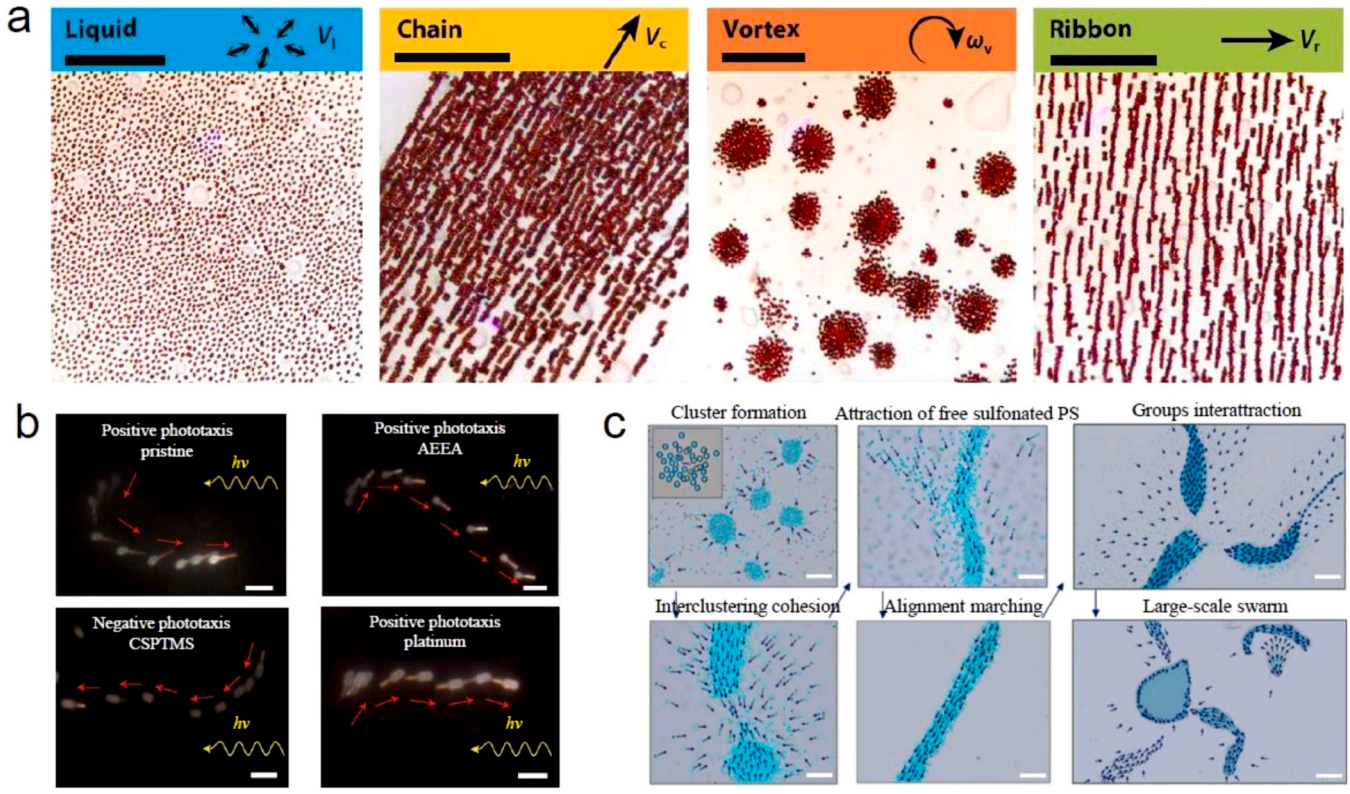

Fig. 5. (a) Multimodal transformation of hematite colloidal particles in liquid, chain, vortex, and ribbon-like swarm states. Scale bars: 50 μm. (b) Superimposed images of sequential frames. The Pristine and AEEA-treated nanotrees migrate in the tail-forward direction and exhibit positive phototaxis. The CSPTMS-treated nanotree migrates in the head-forward direction and exhibits negative phototaxis. The Pt-decorated nanotree migrates in the head-forward direction and exhibits positive phototaxis. Scale bars: 10 μm. (c) The emergence of swarming behavior of ZnO-sulfonated PS mixture: sulfonated PS accumulate around the ZnO nanorod and form clusters with it as the core (inset); cohesion of adjacent ZnO nanorod-sulfonated PS clusters via attractive osmosis; self-alignment of free sulfonated PS and ZnO nanorod-sulfonated PS clusters; alignment marching of clusters; further aggregation of ZnO nanorod-sulfonated PS clusters; large-scale swarming behavior of the ZnO-sulfonated PS mixture.
Reproduced with permission [90]. Copyright 2019, AAAS. (b) Reproduced with permission [91]. Copyright 2016, Springer Nature. (c) Reproduced with permission [92]. Copyright 2021, Springer Nature.

delivery of particles in vitro and in vivo. However, drug conveys to specific disease sites still mainly relies on the circulatory system. Adapting chemotaxis into the drug delivery system would be advantageous in terms of decreasing the therapeutic dosage and reducing collateral cytotoxicity [53].

Chemotaxis can be designed to provide another route for the directional motion control. Somasundar et al. studied the directional control of both positive and negative chemotaxis in liposomal protocells, shown in Fig. 6(d) [97]. The finding indicates that the propulsion mechanism is based on the interaction of enzyme-catalysis-induced positive chemotaxis and solute-phospholipid-based negative chemotaxis. Therefore, controlling the extent and direction of chemotaxis shows significant implications for developing cell mimics and delivering vehicles with motion reconfiguration capability under different environmental conditions [97]. To determine the mechanism for metabolon formation, Zhao et al. studied the coordinated movement of the first four enzymes, including hexokinase, phosphoglucose isomerase, phosphofructokinase, and aldolase of the glycolysis cycle by utilizing microfluidic and fluorescent spectroscopy techniques. The study suggested that each enzyme follows its substrate gradient generated by the previous enzymatic reaction. While subjected to conditions mimicking cytosolic crowding, the observed rate was still similar to the previously reported rate of enzyme diffusion in living cells. Chemotaxis serves as the basis for organizing metabolic networks in the cytosol [98]. These prior studies suggest an unprecedented opportunity for chemotaxis-based directionality control. Thus, the following steps would be the development of synthetic micro- and nanomotors capable of achieving self-targeting and navigation in complex or microenvironments with response to chemical gradient, which integrates sensing, processing, and self-propelling functionalities.

3.2. *Applications of collective behavior of micro/nanorobots*

The environmental remediation applications can be efficiently enhanced by dynamic microswarms motion control due to their high processing efficiency by the collective working mode and sizeable specific area of agents [99,100]. For instance, Zhang et al. developed a swarming biohybrid adsorbent (porous spore@Fe_3O_4) through in situ growing magnetic nanoparticles on hydrothermally-treated fungi spores. Due to porous structuring and high-adsorbing components, it can effectively remove heavy metal ions in contaminated water, shown in Fig. 7(a) [101]. Notably, the enhanced adsorption capacity and shorter removal time were found for such adsorbent by controllably magnetic collective motion when compared to nonmotile counterparts [101]. Sun et al. reported the cooperative behavior of micromagnetic submarines based on sunflower pollen grains (SPGs) and investigated their application in oil and microplastic removal [102]. When the hollow micro submarine swarms stay at the oil-water interface, capillary absorption of oil into the hydrophobic structure is feasible. Fig. 7(b) shows a formed vortexlike microswarm when applying the magnetic field on the top. Under the spinning mode, the micro submarine's swarm becomes a giant vortex, mixing even and accelerating absorption. Compared with static adsorption, dynamic adsorption from the motile vortex is faster and cleaner. Wang et al. developed photocatalytic Au@Ni@TiO_2-based micromotors [103]. As Fig. 7(c) shows, in the mixture of individual

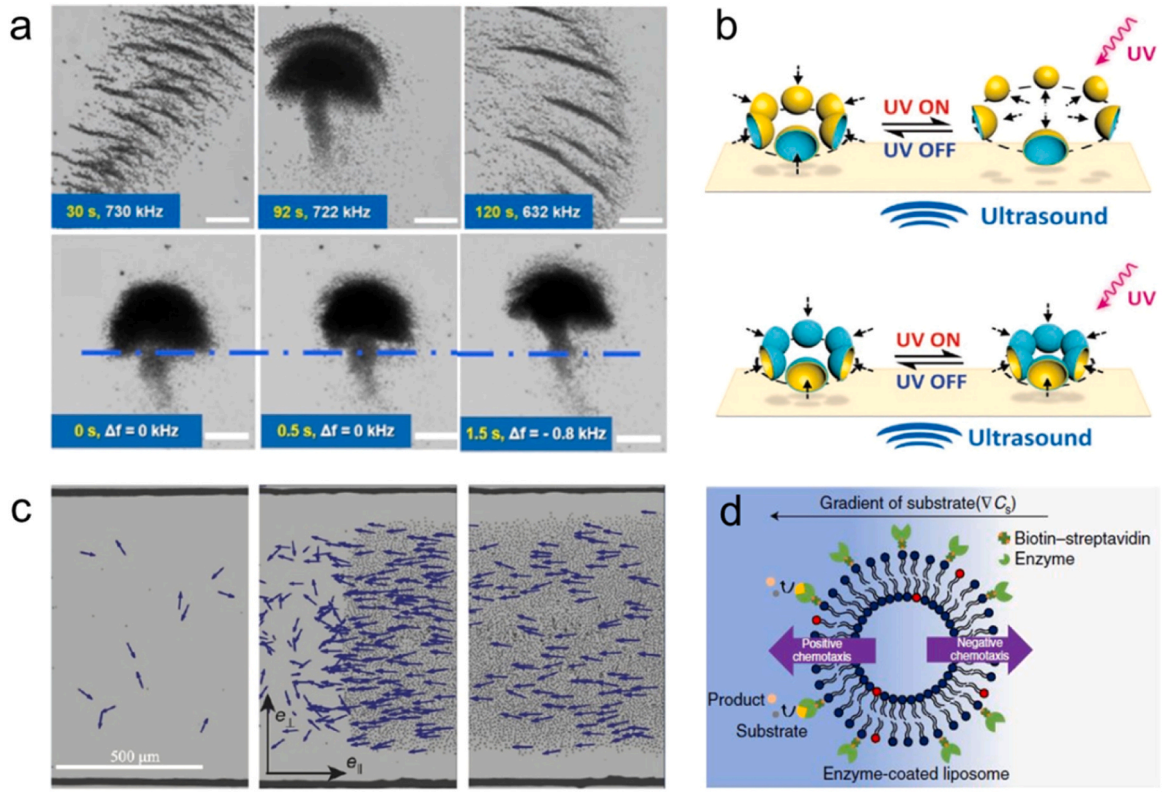

Fig. 6. (a) Time-lapse images of formation and motion of acoustically triggered EGaIn colloidal swarm.(b) Structure-depended collective behavior for the microbowls in a hybrid source of UV light and an acoustic field. The dispersion and compaction behaviors were formed for the resulting swarm of TiO2-Au microbowls and Au-TiO2 microbowls, respectively. Scale bar: 20 μm. Blue surfaces: TiO2, and yellow surfaces: Au. (c) Collective motion of rolling particles from isotropic gas to the propagating band and homogeneous polar liquid at increasing density. Scale bar: 500 μm.(d) Illustration of enzymatic propulsion or solute interactions driving the migration of enzyme-coated liposomes towards or away from the substrate. Egg Liss Rhod PE (the red-headed lipid) serves as a fluorescent marker, while DSPE-PEG (2000) biotin (the blue-headed lipid with attached enzyme) and L-phosphatidylcholine lipids (the blue-headed lipid) make up the rest of the liposomes.
(a) Reproduced with permission [93]. Copyright 2020, Wiley-VCH.(b) Reproduced with permission [94] Copyright 2019, Wiley-VCH. (c)Adapted with permission from ref [96] Copyright 2013 Springer Nature. (d) Reproduced with permission [97] Copyright 2019, Springer Nature.

catalytic Au@Ni@TiO_2 NBs and PS particles, NBs can efficiently collect PS particles through phoretic interactions and transport large numbers. Park et al. demonstrated an efficient method for the removal of glyphosate (GLY) from artificial and real water samples by treating the samples with magnetite nanoparticles (Fe_3O_4 NPs) (Fig. 7(d)) [104]. The Fe_3O_4 NPs, acting as catchers and carriers for magnetic removal, can be covalently bonded with GLY due to their chemical structure. The collected contaminated Fe_3O_4 NPs can be reactivated by thermal treatment, thus it enables the cyclic use of the magnetic absorber [104].

Furthermore, Hu et al. fabricated multilight-responsive micromotors Fe_3O_4 @poly(glycidyl methacrylate)/polystyrene (Fe_3O_4 @PGS) as a platform for performing "chemistry-on-the-fly". It can fulfill diverse tasks by using both the catalytic efficiency of Fe_3O_4 NPs and the immobilized enzyme (lipase) [105]. The swarming motion of the Fe_3O_4 @PGS micromotor led to mixing in the microscale, which boosted the mass exchange in the treated solution. As shown in the left of Fig. 8(a), the catalytic degradation of rhodamine B (RhB) was accelerated by over 10 times under the sunlight. On the other hand, the developed micromotor could further accelerate enzymatic reactions of lipase on Fe_3O_4 @PGS by more than 50%, not only in aqueous solutions but also in organic phases resulting from the right of Fig. 8(a). In addition, Xie et al. realized multiple, desired collective modes within one colloidal system. They applied alternating magnetic fields to program hematite colloidal particles in liquid, chain, vortex, ribbon-like microrobotic swarms and enabled further fast and reversible transformations between them as described previously. Such reconfigurable microrobot swarm can provide versatile collective modes to address environmental variations or multitasking requirements. As shown in Fig. 8(b) (top), the colony-like vortex microrobot swarm was demonstrated to push a PS microsphere whose volume is about 40,000 times of an individual microrobot volume. In addition, the ribbon swarm could perform large-area manipulation in a synchronized manner. However, the carrying ability was less than that of the vortex due to the fluidic flow induced by the ribbon, as shown in Fig. 8(b) (bottom) [90].

In addition, micro/nanoswarms hold great promise in the area of biomedical applications. For example, Law et al. demonstrated magnetic particle swarms to accurately block the blood flow inside a targeted region for selective embolization [106]. Fig. 9(a) illustrates the block of the junctions and the forces exerted on tip particles. The experimental results showed that swarms are split when the magnetic field strength applied was lower than the calculated B critical. Swarms maintained their integrity at a junction when the magnetic field strength applied was higher than the calculated $B_{critical}$. Sun et al. reported a magnetic microswarm platform for biofilm eradication [107]. The active delivery properties of the micro-robotic swarm and the broad-spectrum antimicrobial properties of the magnetic liquid metal droplets are combined to achieve targeted biofilm eradication, shown in Fig. 9(b). The microswarm demonstrated here has great potential for treating bacterial biofilms on medical implants. Wang et al. showed an application of reconfigurable magnetic microswarm for thrombolysis under ultrasound imaging. The process of thrombolysis in blood under ultrasound imaging is shown in Fig. 9(c). The upper three figures schematically illustrate the process, corresponding to the lower experimental results. The blood clot gradually dissolves, resulting in the translational locomotion of the microswarm (t = 30 min). After the clot is dissolved the microswarm reaches the end of the channel (t = 90 min) at a mean velocity of 56

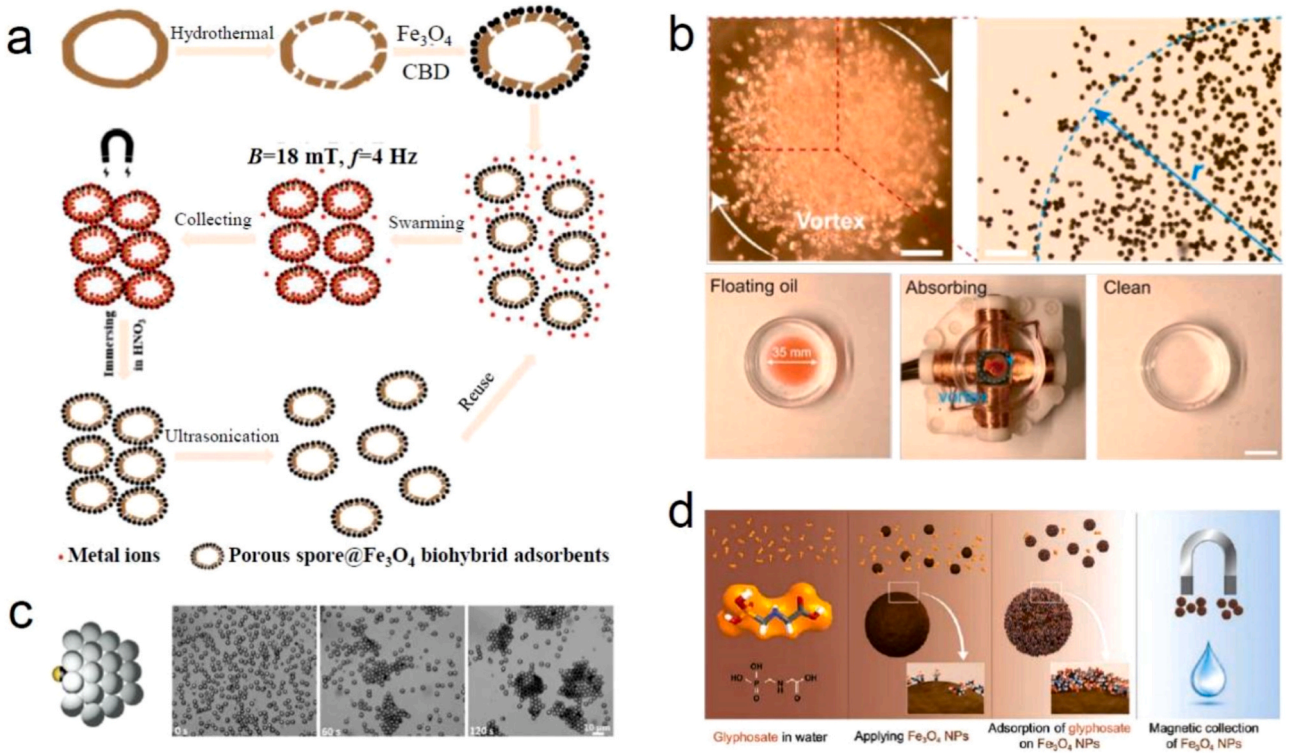

Fig. 7. Environmental remediation of synthetic collective microrobots. (a) Reusable biohybrid adsorbents collectively remove heavy metal ions in an external magnetic field. (b) Removal of micropollutants using reconfigurable cooperative behaviors. Top: the giant vortex at the oil-water interface. Scale bars, 200 μm. Bottom: images showing 100 μ of dyed corn oil absorbed by hollow micro-submarines (10 mg) vortex. (c) Photocatalytic TiO_2 micromotors for removal of microplastics: the schematic illustration and time-lapse optical images of phoretic interaction between TiO_2 micromotor and PS particles. (d) Fe_3O_4 NPs absorb glyphosate herbicide (GLY) molecules in water and their subsequent magnetic collection for recycling.
(a) Reproduced with permission [101]. Copyright 2018, John Wiley and Sons. (b) Reproduced with permission [102]. Copyright 2020, Elsevier B.V. (c) Reproduced with permission [103]. Copyright 2019, American Chemical Society. (d) Reproduced with permission [104]. Copyright 2020, Springer Nature.

$\pm$ 17.3 μm min^{-1}. In the area of antibacterial treatments, Hoop et al. designed Ag-coated magnetic Pd nanocoils to target and kill bacteria [108]. The Pd nanocoils were sequentially coated with Ni and Ag for magnetic manipulation and antibacterial properties, respectively. Analysis by confocal laser scanning microscope (CLSM) confirmed the time-dependent induction of bacterial killing, shown in Fig. 9(d). The results indicate that the Ag-coated nanocoils could be used as the antibacterial mode of action due to thier membrane disintegration ability [108].

With motion control and collective behavior, controlled NBs can be observed and tracked using imaging techniques in vivo. NBs integrated with high resolution imaging techniques are shown, in Fig. 10(a): positron emission tomography (PET), and in Fig. 10(b): in vivo fluorescence images [70,110], respectively. Hortelao et al. used silica nanoparticles containing urease enzymes and gold nanoparticles as nanomotors and reported the swarming behavior of urease-powered nanomotors and their tracking using PET in combination with computed tomography (CT), both in vitro and in vivo, as shown in Fig. 10(a) [70]. Their work shows the collective behavior of nanomotors integrated with PET-CT imaging technique, holding great potential in biomedical applications. Zhang et al. reported a dual-responsive biohybrid neutrophil-based microrobot ("neutrobot") that can actively deliver cargo to malignant glioma [110]. Upper part of Fig. 10(b) schematically illustrates the glioma surgical resection model diagram and active accumulation of neutrobots to inflamed postoperative glioma through magnetic propulsion and chemotaxis. Sequences of images in Fig. 10(b) show in vivo fluorescence signals of glioma-bearing mice (control group), glioma-bearing mice after surgical treatment (chemokine gradient, CG group), glioma-bearing mice treated with rotating magnetic field (RMF group), and glioma-bearing mice after surgical treatment and treated with magnetic field dual response group (DR group). The NBs obtained in this work proved potential applications in both drug delivery and in vivo imaging.

4. Advanced function integration of micro/nanorobots

Nanorobotics ultimate goal is function integration to accomplish more sophisticated tasks. However, effective control of NBs behaviors and interactions similar to biomaterials remains a major challenge. Conventional nano- electronic circuits and mechanical actuators cannot be scaled down to the molecular scale. Therefore, signaling and information processing mechanisms leading to specific behaviors of NBs should be developed.

Self-oscillating gels powered by Belousov-Zhabotinsky (BZ) reaction showed emergent behaviors with various movement transitions controlled by the reactions' kinetic parameters. Nava-Medina et al. combined 3D printing techniques with BZ reaction to investigate the macro-scale patterns observed in nature [111], shown in Fig. 11(a). Inui et al. demonstrated the possibility of reversibly switching the microgel oscillations from an "on" active state of the BZ reaction to an "off" inactive state by changing the temperature in combination with thermoresponsive microgels [112], indicated in Fig. 11(b). Furthermore, Yoshida developed self-oscillating polymer gels with autonomous functions. In contrast to conventional stimuli-responsive gels, the "self-oscillating" polymer gels autonomously undergo periodic swelling/deswelling oscillation without on–off switching of external stimuli in a closed solution, shown in Fig. 11(c) [113]. The motive ability of miniaturized gel robots critically depends on the wavelength of BZ waves. Due to the relatively large wavelength, i.e., larger than 20 mm for Z-Ru(II), the robots with smaller sizes cannot contain a full chemical

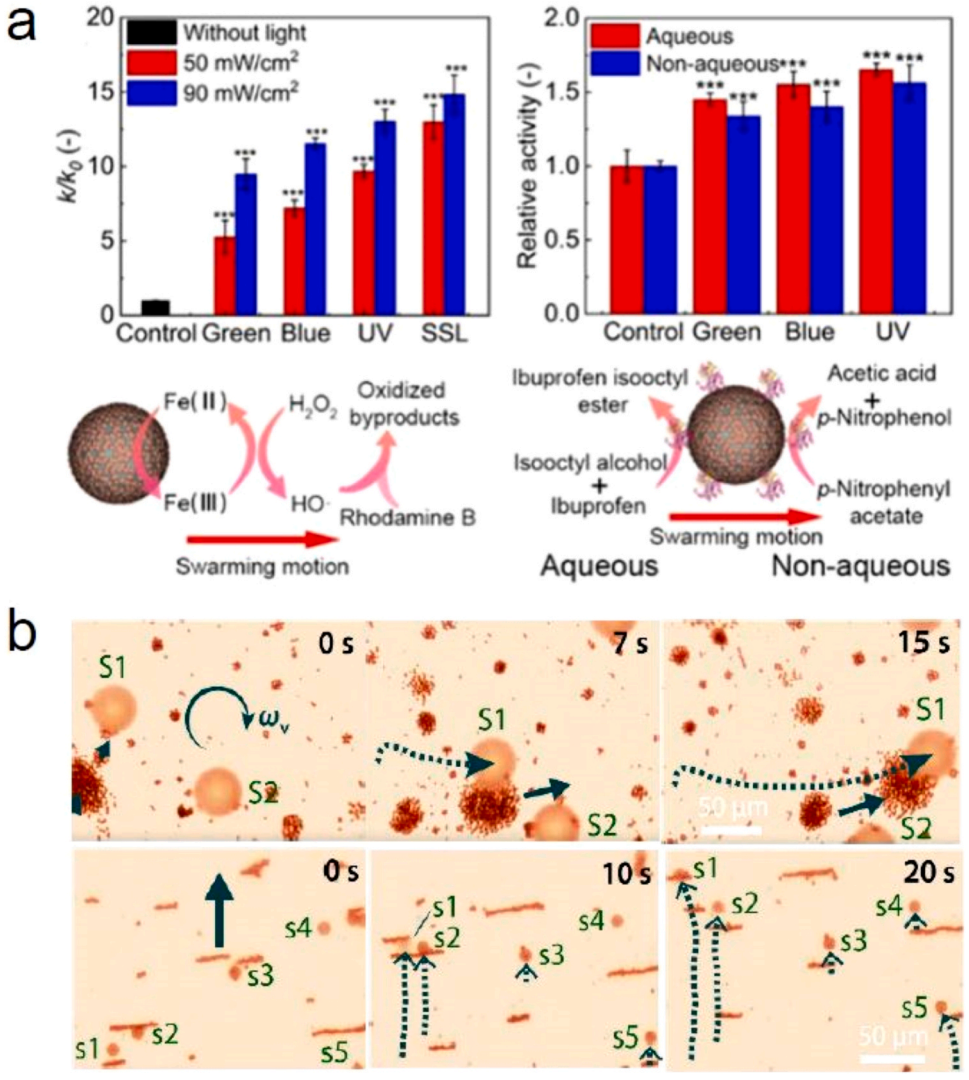

Fig. 8. (a) Micromotor for the acceleration of (bio)chemical reactions. Left: ratio of kinetic constants k of RhB degradation catalyzed by Fe_3O_4 @PGS under green, blue, UV, and simulated sunlight (SSL) irradiation to that of control without light irradiation (k_0); mechanism of the accelerated degradation of RhB. Right: relative enzymatic activities of Fe_3O_4 @PGS-E determined by the hydrolysis of p-NPA (red) and the esterification of ibuprofen (blue) under different lights (90 mW/cm^2); mechanism of the accelerated enzymatic reactions in both aqueous and nonaqueous systems. b) Snapshots showing manipulation of PS microsphere (S_1; diameter, 40 mm) by a vortex swarm (top) and synchronized manipulation of Ag microspheres (marked with s_1 to s_5; diameter, 8 mm) by the ribbon swarm (bottom). (a) Reproduced with permission [105]. Copyright 2020, American Chemical Society.(b) Reproduced with permission [90]. Copyright 2019, AAAS.

wavelength. Epstein's group reported how higher concentrations of organic species and temperature lead to wavelength reduction to 0.4 mm. Alternatively, the reduction of bromate, hydrogen ion, and metal catalyst has been used to achieve shorter wavelengths [114]. Suematsu et al. utilized the BZ reaction product to affect the driving force of a propelled object. Integrating an aqueous droplet with the BZ reaction into an oil phase, including a surfactant, the droplet can self-propel by jumps using chemical waves and the interfacial reaction of the surfactant and bromine (Br_2). In the latter case, bromine is the reaction intermediate and the "fuel", shown in Fig. 11**(d)** [115]. Hayashi's group observed that chemical and mechanical self-oscillations in BZ hydrogels are inherently asynchronous. Experimentally, there is a noticeable delay in swelling–deswelling response after a change in the chemical redox state. Such delay can be attributed to the fact that the swelling response to oxidation is shorter than the deswelling response to reduction [116].

Soft chemical robots fabricated from a polymer, including a cyclic reaction network operating as a metabolism, have been shown. The soft robot is actuated by swelling and deswelling of polymer, driven by BZ reaction. Hashimoto's group used ruthenium(II) tris(2,2′-bipyridine) (Ru(bpy)32 + BZ catalyst covalently bonded to the polymer chain of N-isopropyl acrylamide (NIPAAm). The diffusion of the substrate actuates the robot into the gel matrix in aqueous solutions with an added substrate. Hydrophilic 2-acrylamide-2-methylpropane sulfonic acid was co-polymerized into the gel region to achieve anisotropic expansion and contraction [117]. Huck and co-workers demonstrated more complex responsive hydrogels by employing an enzymatic reactions network. Trypsin enzyme has been used to activate the reaction network of the motor. It was shown that the trigger concentration and the influence of kinetic rate constants could be used to develop a computational model for predicting materials' responses [118]. Chemical reaction networks can be responsible for multiple processes in biomaterials, including chemotaxis, circadian rhythms, and the firing of nerve cells. Whitesides' group demonstrated a reactions network using amide formation, thiolate-thioester exchange, thiolate-disulfide interchange, and conjugate addition leading to oscillated behaviors and bi-stability in organic thiols and amides [119].

Fast swelling/deswelling and dispersing/flocculating oscillations of autonomously oscillating hydrogel microspheres (microgels) at periods of single-order seconds were accomplished. The design of the oscillating

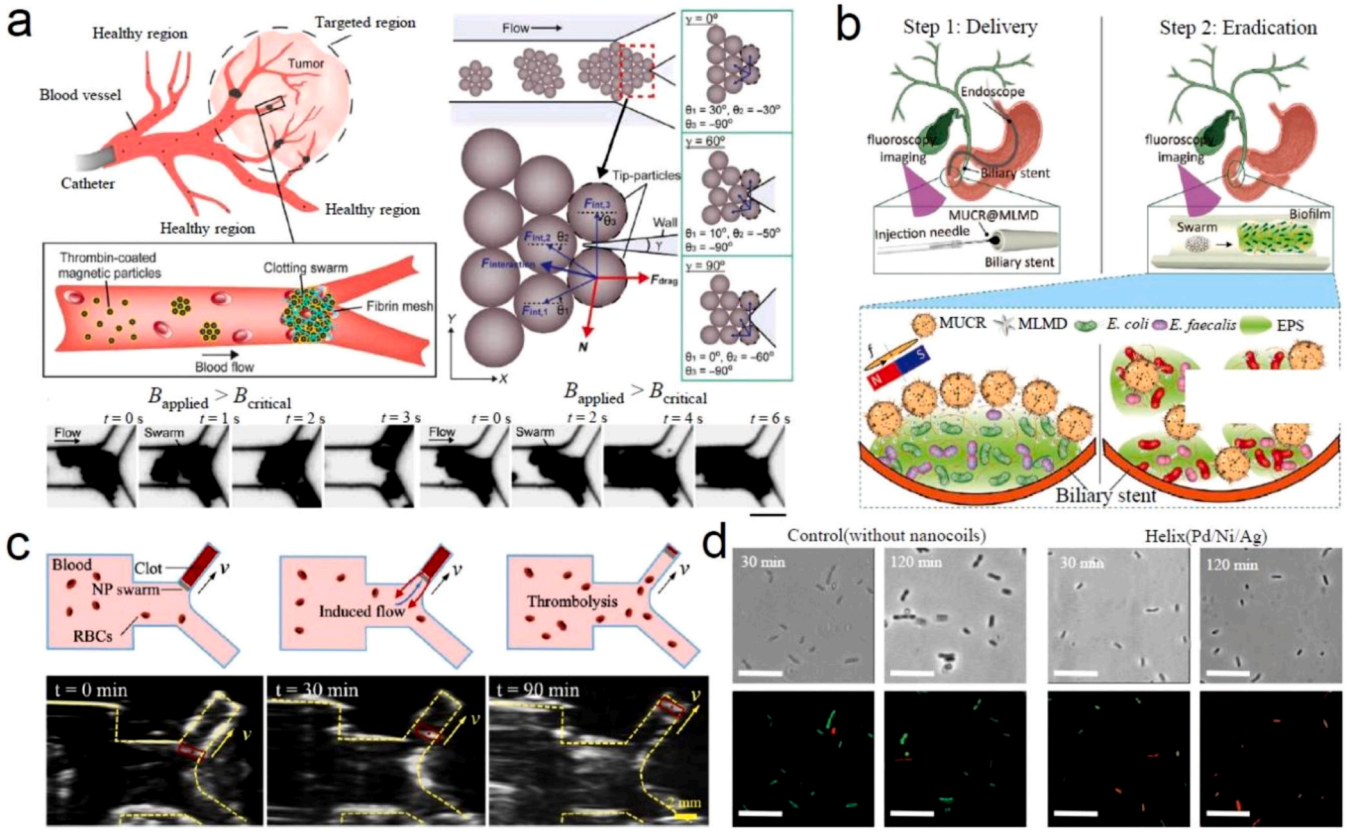

Fig. 9. (a) Schematics illustrating using magnetic particle swarms to block the junctions inside a targeted region. Analysis of the forces exerted on tip particles. The brown circles indicate magnetic particles. Experimental validations for the model. The integrity of swarms when the magnetic field strength applied was lower and higher than (critical magnetic field intensity) $B_{critical}$, respectively. Scale bar, 20 μm. (b) Schematic diagram of the eradication of biofilm adhered to biliary stents using the MUCR@MLMDs swarm. (c) Biomedical applications of synthetic collective microrobots for thrombolysis. (d) CLSM images of E. coli incubated with 50 ppm by LIVE/DEAD Bac Light bacterial viability assay. Bacterial cells with intact membranes are stained green, and bacteria with compromised membranes are stained orange or red. Scale bars, 10 μm.
(a) Reproduced with permission [106]. Copyright 2022, AAAS. (b) Reproduced with permission [107]. Copyright 2022, John Wiley & Sons. (c) Reproduced with permission [109]. Copyright 2020, IEEE. (d) Reproduced with permission [108] Copyright 2015, John Wiley and Sons.

microgels is based on incorporating neutral and hydrophilic acrylamide monomers into conventional microgels to suppress the irreversible aggregation of the microgels during oscillation at high substrate concentrations and high temperatures in the BZ reaction. In contrast to conventional microgels, the microgels mentioned above can carry out the BZ reaction under optimized conditions without irreversible aggregation at higher temperatures, resulting in short oscillation periods (~7 s) that were obtained from optical transmittance measurements. Furthermore, a macrogel composed of organized microgels was prepared, showing a high-speed swelling/deswelling oscillation (oscillation period: ~23 s). This new oscillating microgel has high potential in advanced materials, e.g., autonomously oscillating micropumps that imitate the human heartbeat [120].

5. Cell-level biomedical applications of micro/nanorobots

Micro/nanorobots hold promising potential in the area of minimally invasive treatments. Theranostic, non-toxic, non-immunogenic, biocompatible, and biodegradable NBs with a high surface area can comprise various organic and synthetic materials for such targeted biomedical applications. For example, gold nanoparticle-based nanorobots (Au-NBs) have shown excellent biocompatibility, biofunctionalization, optically tunable characteristics, and physicochemical stability [121,122]. The solid-state and organic nanoparticles, such as those made of proteins, can be prepared using fibroins, albumin, gelatin, gliadine, legumin, lipoprotein, and ferritin using emulsion, nano-spray drying, electrospraying, and desolvation methods [123, 124]. Biodegradable poly(lactic-co-glycolic acid) (PLGA) nanoparticles can be used to target specific organs, tissue, or cells [125]. Au-NBs conjugates have been applied in gene delivery and RNA-interference procedures [126]. In photodynamic therapy (PDT), light and photosensitizing chemical agents can be applied to elicit cell death. PDT has been proven effective inactivating pathogens, tumors, and viral infections [127].

NBs can cross the cellular membrane by diffusion, adhesion to the cell membrane, and internalization. Cell uptake can be programmed using specific surface coatings, hydrophobicity, therapeutic agents, targeting ligands, imaging parts, and drugs, which alter NBs' physical, chemical, and biological properties. After entry into physiological fluids, the surface of nanoparticles' surface adsorbs salts, ions, lipids, vitamins, and proteins. Cells respond to nanoparticles,' and the invasion depends on NBs' size, shape, functionalization, and physicochemical properties [128,129]. NBs' surface modification and shape/aspect ratio is another parameter for controllable NBs uptake by cells. Surface adsorption and cellular uptakes of NBs can be increased by specific substances [130], for example, amino groups, such as poly(vinyl alcohol-co-N-vinylamine) copolymers [131]. Nanocarrier design combined with pulmonary drug delivery has the potential of immune-engineering approaches to targeting and activating immune cells in the lung by nanocarriers [132]. It was reported that nanorods with an aspect ratio above five were preferentially endocytosed by epithelial cells. In contrast, there was a lack of shape-dependent uptake following exposure to macrophages in vitro

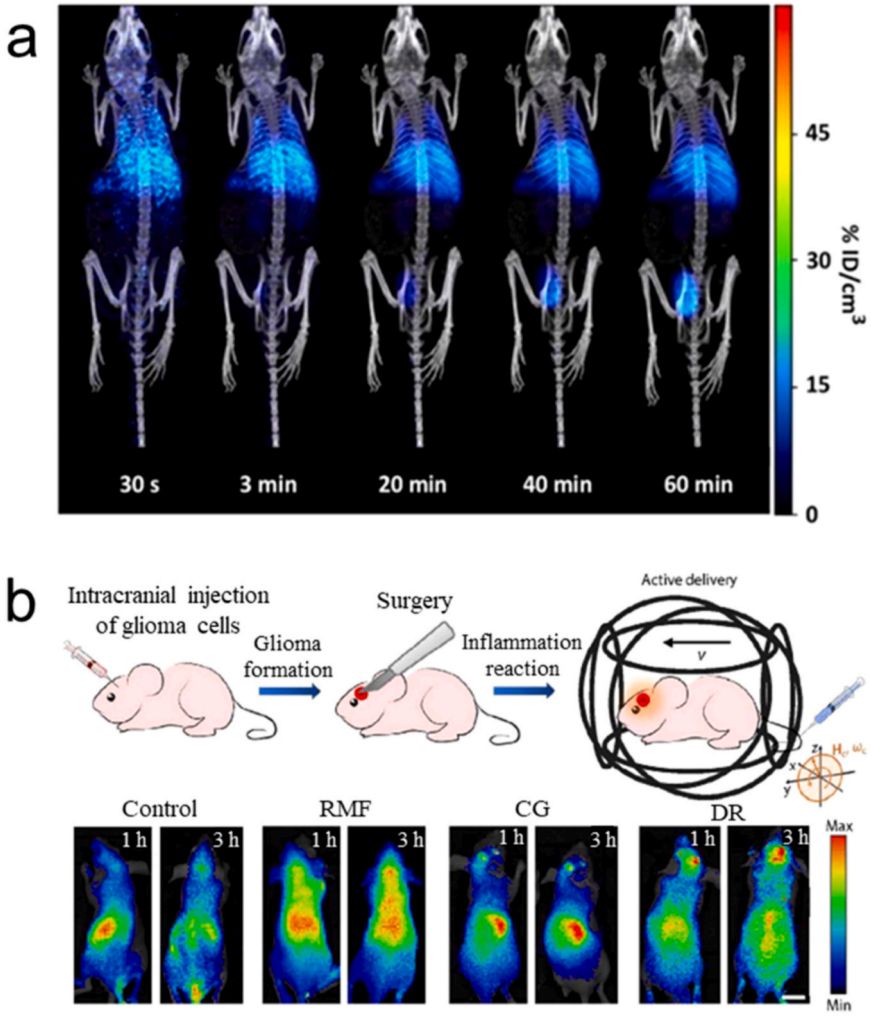

Fig. 10. (a) PET-CT images (maximum intensity projections, coronal views) were obtained at different time points after intravenous administration of ^{18}F-labeled urease-AuNP nanomotors. (b) Upper schematic diagram is the process of the glioma surgical resection model and active accumulation of neutrobots to inflamed postoperative glioma through magnetic propulsion and chemotaxis. Below are in vivo fluorescence images of different treatment groups.
Reproduced with permission [70]. Copyright 2021, AAAS. (b) Reproduced with permission [110]. Copyright 2021, AAAS.

[133]. Dynamics of particles' uptake by cells and translocation across tissue membranes have been demonstrated with a time-lapse fluorescence imaging technique, enabling direct visualization of various cells up to 24 h [134]. Nanoparticles can be tested in vivo for potential therapeutic applications. For example, interactions of polymer-coated GNPs with B cells and their functions in mice have been reported [135]. Nanoparticles can also be used as nanotools to probe the cell mechanics (adhesion, cytoskeleton, stiffness, and motility), rheological properties, and mechanotransduction [136,137]. Another subclass is active nanoparticles that integrate natural taxes and can be controlled externally as nanomotors [138].

New microfluidic techniques offered high-throughput isolation, screening, sorting, and diagnostics of single cells and reagents in droplets/capsules with volumes in the range from 10^{-6} to 10^{-15} L generated at kilohertz frequencies [139]. Encapsulated cells in fluidic cores have tiny liquid compartments, where metabolic molecules accumulate fast, leading to early detection, identification, and screening of thousands of reactions [140,141]. Generated droplets separated by immiscible phase represent a test tube or a microscale reactor to mix compartments by diffusion, conduct assays, and reactions rapidly microfluidics can be coupled with other analytic methods (e.g., fluorescence, mass spectrometry, electrochemistry) can be used to conduct millions of screening tests of cells collected from patients [142]. The high throughput enables research of multiple cells to describe the heterogeneous population of cells precisely, find rare cell types, and determine hits in a directed evolution [143].

In normal conditions, the cell's membrane has low permeability to polar objects. Using electrical stimulation of nanocarriers – cell system, drugs, DNA, RNA, proteins, dyes, peptides, and amino acids can be delivered to tissue and cells using iontophoresis, electroporation, and electrophoresis. Iontophoretic drug delivery has recently been used as a novel method for cancer treatment in vivo [144]. Electroporation is an electro-physical approach to perform molecular transfections to cells upon application of an electric field, shown in Fig. 12 [145,146]. The uptake of small molecules (e.g., dyes), DNA plasmids, interfering RNAs, and nanoparticles have been broadly examined on different types of mammalian cells, yeast, and bacteria [147]. Solution containing DNA was injected in droplets leading to efficient electroporation by the voltage applied to passing cells [148]. Nanoparticle-based chemotherapeutics in electroporation showed advantages to overcome desmoplastic chemoresistance [149]. Clinical results demonstrated that the immunogenicity of DNA vaccines could be significantly improved if delivered with electroporation [150]. Another example showed that samples comprising up to 500 million T cells had been processed at 20 million cells/min to produce autologous therapies [151]. Compared to conventional electroporation devices, microfluidic (microscale)

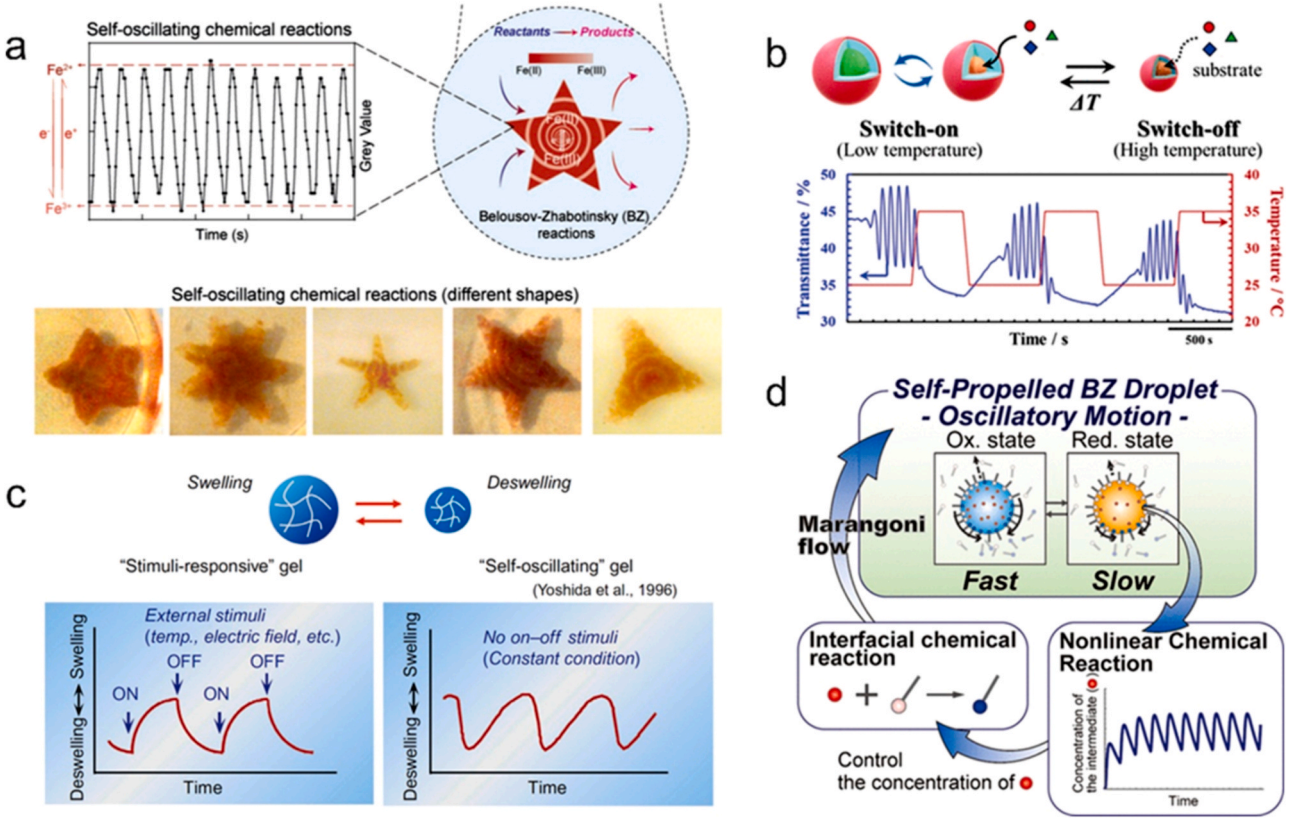

Fig. 11. Function integration in NBs using reaction networks, self-oscillating, and stimuli-responsive materials systems. (a) Different confined shapes were formed by the BZ reaction through extrusion-based 3D printing method. Iron (Fe) dynamically shifts from a 2^+ (reduced; Fe(II)) to the 3^+ (oxidized; Fe(III)) state, producing a continuous pigmentation change (red to transparent). (b) The reversibly switch the microgel oscillations from an "on" active state of the BZ reaction to an "off" inactive state by changing the temperature in combination with thermoresponsive microgels. (c) Stimuli-responsive and self-oscillating gels. (d) The illustration of the relationship between the BZ reaction and self-propelled motion.
(a) Reproduced with permission [111]. Copyright 2021, John Wiley & Sons. (b) Reproduced with permission [112]. Copyright 2020, American Chemical Society. (c) Reproduced with permission [115] Copyright 2016, American Chemical Society

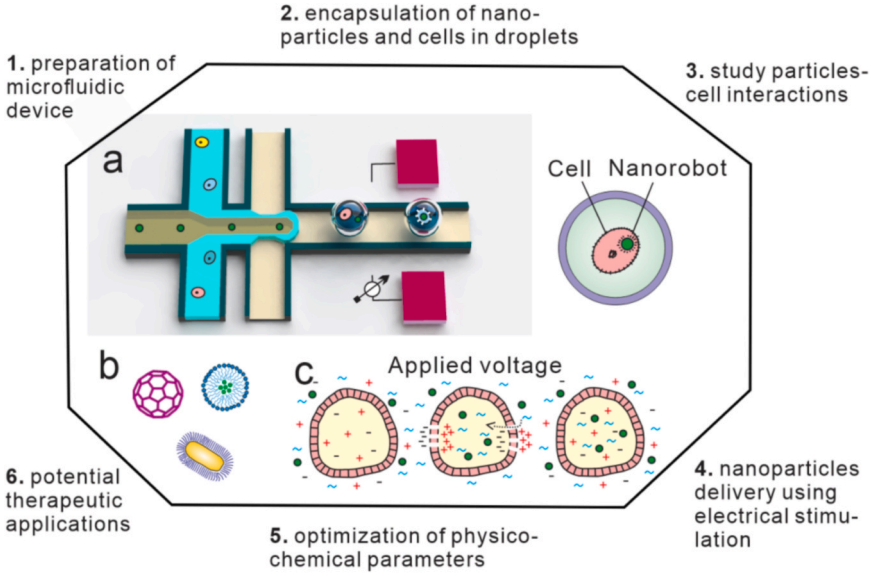

Fig. 12. Application of droplet microfluidics to deliver active nanoparticles in biological cells. (a) Schematic image of a microfluidic device for encapsulation of nanoparticles with biological cells. (b) Schematic image of nanoparticles with various morphology, aspect ratio, and surface coatings. (c) Controllable delivery of active nanoparticles in a cell using electroporation.

electroporation devices have advantages such as higher cell viability rate, high transfection efficiency, lower sample contamination, and smaller Joule heating, shown in Fig. 12(a). Microfluidic devices with integrated micro-electrodes can be used for highly-parallel biological cell electroporation under low voltage (< 1 V; for example, HeLa cells with transmembrane potential around 0.5 V) [152]. Subsequently, cells' uptake of nanoparticles with various size, morphology, aspect ratio and functionalization (Fig. 12(b)) can be studied on-chip under electrical stimulation, illustrated in Fig. 12(c).

6. Conclusions and outlook

Next nano -and microrobots combine capabilities accumulated during past decades. NBs with tailored properties, including negligible inertia, ultra-fast motion, precise positioning, high strength-to-weight ratio, and high-efficiency in energy conversion are of high interest for multi-tasks. The field started from curiosity-driven research and the first applications of solid-state NBs, including delivery of cargo payloads, environmental remediation, drugs delivery, isolation of pathogens, and minimally-invasive surgery. Further development of nanorobotics faced difficulties, such as challenges in achieving the required biodegradability and biocompatibility. The utilization of the microfluidics technique has shown great promise in fabricating multifunctional NBs, given its advantage for low-cost, high-yield production. In addition, it provided precise control and manipulation of the geometric characteristics and functions of NBs. Thus, microfluidics serves as an emerging and promising tool in the biomedical field. The next critical step in developing microfluidics-based NBs concerns the integration of functions. It would be ground-breaking to broaden and optimize the performance of NBs for biosensing and lab-on-chip applications.

The field of nanorobotics faced difficulties due to the inability to scale down sophisticated electronic and mechanical parts. The next generation of NBs can likely be built based on biomimetic information processing circuits and processes, which require establishing chemical networks leading to specific functions. Understanding how reaction networks can be integrated is a hot interdisciplinary topic for achieving responsive and intelligent NBs. Since microfluidics has succeeded in screening of millions of reactions, e.g., during the discovery of drugs, the same techniques can be applied to identify coupling conditions and study responses of NBs. It is known that a combination of some reactions can form bistable and oscillating networks (if coupled to energy-feeding systems). Subsequently, the next study can concentrate on research of networks' adaptation, evolution, and responses, such as chemotaxis. Another advantages, using microfluidics, observing phenomena take place much faster than on a macroscale. For example, molecules' traffic and mixing time in a biological cell is on the order of microsecond. In addition, microfluidics can be used to encapsulate various "metabolic blocks" or coupled cycles, leading to advanced NBs.

During past years, the convergence of classical drug delivery using nanoparticles and active NBs is observed. Interactions among active NBs and biological cells using droplet microfluidics is a rapidly evolving research area. Nanoparticles with specific sizes, shapes, flexibility, aspect ratios, and surface chemistry have been designed for on-demand uptake by biological cells. Subsequently, nanoparticles' toxicity and therapeutic applications can be studied. It is essential to mention that in some instances, conventional medicine experience difficulties in delivering passive nanoparticles, therapeutics, or drugs into cells. In this scenario, NBs can be used to penetrate living cells' membrane without damaging viable functions. For example, biocatalytic reactions, ultrasound, iontophoresis, electrophoresis, and electroporation are the main methods, which can be used to deliver NBs in cells and tissue. Iontophoresis is used to guide molecular species and ions through the bloodstream and organs. However, it is challenging to penetrate the cellular membrane. In the next step, electroporation or short voltage pulses are used. In addition, droplet microfluidics in combination with electroporation provides research tools to deliver NBs into cells at significantly lower voltages. Subsequently, interactions of NBs with individual cells and simultaneous screening of vast populations of cells can be studied. Undoubtedly, the field of next wireless nanorobotics integrating remote control, reactions networks, programmable responses, and biomedical tools have bright prospects in the future.

Declaration of Competing Interest

The authors declare that they have no known competing financial interests or personal relationships that could have appeared to influence the work reported in this paper.

Acknowledgements

This work is supported by the National Key Technologies R&D Program of China (2021YFA0715302 and 2021YFE0191800), the National Natural Science Foundation of China (61975035 and 52150610489), and the Science and Technology Commission of Shanghai Municipality (22ZR1405000).

References

[1] A.C. Balazs, P. Fischer, A. Sen, Intelligent nano/micromotors: using free energy to fabricate organized systems driven far from equilibrium, Acc. Chem. Res. 51 (2018), 2979–2979.
[2] Y. Dong, L. Wang, J. Wang, S. Wang, Y. Wang, D. Jin, P. Chen, W. Du, L. Zhang, B.-F. Liu, Graphene-based helical micromotors constructed by "microscale liquid rope-coil effect" with microfluidics, ACS Nano 14 (2020) 16600–16613.
[3] Y. Yu, J. Guo, M. Zou, L. Cai, Y. Zhao, Micromotors from microfluidics, Chem. Asian J. 14 (2019) 2417–2430.
[4] Z. Wang, Z. Xu, B. Zhu, Y. Zhang, J. Lin, Y. Wu, D. Wu, Design, fabrication and application of magnetically actuated micro/nanorobots: a review, Nanotechnology 33 (2022), 152001.
[5] H. Ning, Y. Zhang, H. Zhu, A. Ingham, G. Huang, Y. Mei, A.A. Solovev, Geometry design, principles and assembly of micromotors, Micromachines 9 (2018) 75.
[6] G. Celik Cogal, P.K. Das, G. Yurdabak Karaca, V.R. Bhethanabotla, A. Uygun Oksuz, Fluorescence detection of miRNA-21 using Au/Pt bimetallic tubular micromotors driven by chemical and surface acoustic wave forces, ACS Appl. Bio Mater. 4 (2021) 7932–7941.
[7] Y. Yang, X. Arqué, T. Patiño, V. Guillerm, P.-R. Blersch, J. Pérez-Carvajal, I. Imaz, D. Maspoch, S. Sánchez, Enzyme-powered porous micromotors built from a hierarchical micro- and mesoporous UiO-type metal–organic framework, J. Am. Chem. Soc. 142 (2020) 20962–20967.
[8] Y. Zhang, H. Zhu, W. Qiu, Y. Zhou, G. Huang, Y. Mei, A.A. Solovev, Carbon dioxide bubble-propelled microengines in carbonated water and beverages, Chem. Commun. 54 (2018) 5692–5695.
[9] S. Naeem, F. Naeem, M. Manjare, F. Liao, V.A. Bolaños Quiñones, G.S. Huang, Y. Li, J. Zhang, A.A. Solovev, Y.F. Mei, Tubular catalytic micromotors in transition from unidirectional bubble sequences to more complex bidirectional motion, Appl. Phys. Lett. 114 (2019), 033701.
[10] S. Sanchez, A.A. Solovev, S. Schulze, O.G. Schmidt, Controlled manipulation of multiple cells using catalytic microbots, Chem. Commun. 47 (2010) 698–700.
[11] M. Medina-Sánchez, V. Magdanz, L. Schwarz, H. Xu, O.G. Schmidt, Spermbots: concept and applications, in: M. Mangan, M. Cutkosky, A. Mura, P.F.M. J. Verschure, T. Prescott, N. Lepora (Eds.), Biomimetic and Biohybrid Systems Lecture Notes in Computer Science, Springer International Publishing, 2017, pp. 579–588.
[12] W. Xi, A.A. Solovev, A.N. Ananth, D.H. Gracias, S. Sanchez, O.G. Schmidt, Rolled-up magnetic microdrillers: towards remotely controlled minimally invasive surgery, Nanoscale 5 (2013) 1294–1297.
[13] J. Wu, S. Balasubramanian, D. Kagan, K.M. Manesh, S. Campuzano, J. Wang, Motion-based DNA detection using catalytic nanomotors, Nat. Commun. 1 (2010) 36.
[14] S. Campuzano, J. Orozco, D. Kagan, M. Guix, W. Gao, S. Sattayasamitsathit, J. C. Claussen, A. Merkoçi, J. Wang, Bacterial isolation by lectin-modified microengines, Nano Lett 12 (2012) 396–401.
[15] Z. Wu, J. Troll, H.-H. Jeong, Q. Wei, M. Stang, F. Ziemssen, Z. Wang, M. Dong, S. Schnichels, T. Qiu, et al., A swarm of slippery micropropellers penetrates the vitreous body of the eye, Sci. Adv. 4 (2018), eaat4388.
[16] H. Xu, M. Medina-Sánchez, W. Zhang, M.P.H. Seaton, D.R. Brison, R. J. Edmondson, S.S. Taylor, L. Nelson, K. Zeng, S. Bagley, et al., Human spermbots for patient-representative 3D ovarian cancer cell treatment, Nanoscale 12 (2020) 20467–20481.
[17] V. de la Asunción-Nadal, B. Jurado-Sánchez, L. Vázquez, A. Escarpa, Near infrared-light responsive WS2 microengines with high-performance electro- and photo-catalytic activities, Chem. Sci. 11 (2019) 132–140.
[18] J.A. Tejeda-Rodríguez, A. Núñez, F. Soto, V. García-Gradilla, R. Cadena-Nava, J. Wang, R. Vazquez-Duhalt, Virus-based nanomotors for cargo delivery, ChemNanoMat 5 (2019) 194–200.

[19] B. Zhang, G. Huang, L. Wang, T. Wang, L. Liu, Z. Di, X. Liu, Y. Mei, Rolled-up monolayer graphene tubular micromotors: enhanced performance and antibacterial property, Chem. Asian J. 14 (2019) 2479–2484.
[20] Y. Yuan, C. Gao, D. Wang, C. Zhou, B. Zhu, Q. He, Janus-micromotor-based on–off luminescence sensor for active TNT detection, Beilstein J. Nanotechnol. 10 (2019) 1324–1331.
[21] M. Sun, X. Fan, X. Meng, J. Song, W. Chen, L. Sun, H. Xie, Magnetic biohybrid micromotors with high maneuverability for efficient drug loading and targeted drug delivery, Nanoscale 11 (2019) 18382–18392.
[22] F. Soto, E. Karshalev, F. Zhang, B. Esteban Fernandez de Avila, A. Nourhani, J. Wang, Smart materials for microrobots, Chem. Rev. 122 (2022) 5365–5403.
[23] J. Li, M. Pumera, 3D printing of functional microrobots, Chem. Soc. Rev. 50 (2021) 2794–2838.
[24] J. Sun, H. Tan, S. Lan, F. Peng, Y. Tu, Progress on the fabrication strategies of self-propelled micro/nanomotors, JCIS Open 2 (2021), 100011.
[25] J. Ou, K. Liu, J. Jiang, D.A. Wilson, L. Liu, F. Wang, S. Wang, Y. Tu, F. Peng, Micro-/nanomotors toward biomedical applications: the recent progress in biocompatibility, Small 16 (2020), 1906184.
[26] X. Lin, B. Xu, H. Zhu, J. Liu, A. Solovev, Y. Mei, Requirement and development of hydrogel micromotors towards biomedical applications, Research 2020 (2020), 7659749, 2020/.
[27] S. Ghosh, F. Mohajerani, S. Son, D. Velegol, P.J. Butler, A. Sen, Motility of enzyme-powered vesicles, Nano Lett 19 (2019) 6019–6026.
[28] H. Zhu, S. Nawar, J.G. Werner, J. Liu, G. Huang, Y. Mei, D.A. Weitz, A.A. Solovev, Hydrogel micromotors with catalyst-containing liquid core and shell, J. Phys.: Condens. Matter 31 (2019), 214004.
[29] J. Mujtaba, J. Liu, K.K. Dey, T. Li, R. Chakraborty, K. Xu, D. Makarov, R. A. Barmin, D.A. Gorin, V.P. Tolstoy, et al., Micro-bio-chemo-mechanical-systems: micromotors, microfluidics, and nanozymes for biomedical applications, Adv. Mater. 33 (2021), 2007465.
[30] L.L.A. Adams, D. Lee, Y. Mei, D.A. Weitz, A.A. Solovev, Nanoparticle-shelled catalytic bubble micromotor, Adv. Mater. Interfaces 7 (2020), 1901583.
[31] Y. Liu, Y. Cheng, C. Zhao, H. Wang, Y. Zhao, Nanomotor-derived porous biomedical particles from droplet microfluidics, Adv. Sci. 9 (2022), 2104272.
[32] H. Liu, Y. Wang, H. Wang, M. Zhao, T. Tao, X. Zhang, J. Qin, A droplet microfluidic system to fabricate hybrid capsules enabling stem cell organoid engineering, Adv. Sci. 7 (2020), 1903739.
[33] Y. Feng, X. Chang, H. Liu, Y. Hu, T. Li, L. Li, Multi-response biocompatible Janus micromotor for ultrasonic imaging contrast enhancement, Appl. Mater. Today 23 (2021), 101026.
[34] Y. Yu, J. Guo, Y. Wang, C. Shao, Y. Wang, Y. Zhao, Bioinspired helical micromotors as dynamic cell microcarriers, ACS Appl. Mater. Interfaces 12 (2020) 16097–16103.
[35] T. Liu, L. Xie, C.-A.H. Price, J. Liu, Q. He, B. Kong, Controlled propulsion of micro/nanomotors: operational mechanisms, motion manipulation and potential biomedical applications, Chem. Soc. Rev. 51 (2022) 10083–10119.
[36] W.Z. Teo, M. Pumera, Motion control of micro-/nanomotors, Chem. Eur. J. 22 (2016) 14796–14804.
[37] Q. Yang, L. Xu, W. Zhong, Q. Yan, Y. Gao, W. Hong, Y. She, G. Yang, Recent advances in motion control of micro/nanomotors, Adv. Intell. Syst. 2 (2020), 2000049.
[38] T.R. Kline, W.F. Paxton, T.E. Mallouk, A. Sen, Catalytic nanomotors: remote-controlled autonomous movement of striped metallic nanorods, Angew. Chem. Int. Ed. 44 (2005) 744–746.
[39] M. Liu, L. Pan, H. Piao, H. Sun, X. Huang, C. Peng, Y. Liu, Magnetically actuated wormlike nanomotors for controlled cargo release, ACS Appl. Mater. Interfaces 7 (2015) 26017–26021.
[40] N. Kukreja, V.K. Sharma, Optimal path planning of mobile nanobots navigation control in human physiological systems using advanced soft computing technique, Mater. Today: Proc. 45 (2021) 3426–3430.
[41] J. Zheng, S.H. Lam, H. Huang, L. Shao, Recent progress in optical-resonance-assisted movement control of nanomotors, Adv. Intell. Syst. 2 (2020), 1900160.
[42] J. Wang, Z. Xiong, J. Zheng, X. Zhan, J. Tang, Light-driven micro/nanomotor for promising biomedical tools: principle, challenge, and prospect, Acc. Chem. Res. 51 (2018) 1957–1965.
[43] R. Dong, Y. Cai, Y. Yang, W. Gao, B. Ren, Photocatalytic micro/nanomotors: from construction to applications, Acc. Chem. Res. 51 (2018) 1940–1947.
[44] S. Yu, Y. Cai, Z. Wu, Q. He, Recent progress on motion control of swimming micro/nanorobots, VIEW 2 (2021), 20200113.
[45] H. Manoharan, Y. Teekaraman, R. Kuppusamy, A. Radhakrishnan, K. Hariprasath Venkatachalam, Acclimatization of nanorobots in medical applications using the artificial intelligence system with the data transfer approach, Wirel. Commun. Mob. Comput. 2022 (2022) 1–8.
[46] M. Wang, X. Li, F. He, J. Li, H.-H. Wang, Z. Nie, Advances in designer DNA nanorobots enabling programmable functions, ChemBioChem 23 (2022), e202200119.
[47] W. Xu, H. Qin, H. Tian, L. Liu, J. Gao, F. Peng, Y. Tu, Biohybrid micro/nanomotors for biomedical applications, Appl. Mater. Today 27 (2022), 101482.
[48] M. Wan, T. Li, H. Chen, C. Mao, J. Shen, Biosafety, functionalities, and applications of biomedical micro/nanomotors, Angew. Chem. Int. Ed. 60 (2021) 13158–13176.
[49] H. Choi, J. Yi, S.H. Cho, S.K. Hahn, Multifunctional micro/nanomotors as an emerging platform for smart healthcare applications, Biomaterials 279 (2021), 121201.
[50] Y. Feng, M. An, Y. Liu, M.T. Sarwar, H. Yang, Advances in chemically powered micro/nanorobots for biological applications: a review, Adv. Funct. Mater. 33 (2023), 2209883.
[51] K. Hou, Y. Zhang, M. Bao, Y. Liu, J. Wang, C. Xin, Z. Wei, H. Zhang, Z. Wu, Z. Wang, Biosafety of micro/nanomotors towards medical application, Mater. Adv. 2 (2021) 3441–3458.
[52] C.C. Mayorga-Martinez, J. Vyskočil, F. Novotný, P. Bednar, D. Ruzek, O. Alduhaish, M. Pumera, Collective behavior of magnetic microrobots through immuno-sandwich assay: On-the-fly COVID-19 sensing, Appl. Mater. Today 26 (2022), 101337.
[53] K. Gentile, A. Somasundar, A. Bhide, A. Sen, Chemically powered synthetic "living" systems, Chemistry 6 (2020) 2174–2185.
[54] H. Wang, M. Pumera, Fabrication of micro/nanoscale motors, Chem. Rev. 115 (2015) 8704–8735.
[55] L. Hu, N. Wang, K. Tao, Catalytic micro/nanomotors: propulsion mechanisms, fabrication, control, and applications, in: T. Shabatina, V. Bochenkov (Eds.), Smart Nanosystems for Biomedicine, Optoelectronics and Catalysis, IntechOpen, 2020.
[56] K. Zhang, Y. Ren, T. Jiang, H. Jiang, Flexible fabrication of lipophilic-hydrophilic micromotors by off-chip photopolymerization of three-phase immiscible flow induced Janus droplet templates, Anal. Chim. Acta 1182 (2021), 338955.
[57] A. Chen, X. Ge, J. Chen, L. Zhang, J.-H. Xu, Multi-functional micromotor: microfluidic fabrication and water treatment application, Lab Chip 17 (2017) 4220–4224.
[58] Z. Feng, B. Zhou, X. Su, T. Wang, S. Guo, H. Yang, X. Sun, One-step fabrication of multiphasic Janus microparticles with programmed degradation properties based on a microfluidic chip, Mater. Des. 225 (2023), 111516.
[59] W. Liu, H. Ge, Z. Gu, X. Lu, J. Li, J. Wang, Electrochemical deposition tailors the catalytic performance of MnO2-based micromotors, Small 14 (2018), 1802771.
[60] J. Li, S. Sattayasamitsathit, R. Dong, W. Gao, R. Tam, X. Feng, S. Ai, J. Wang, Template electrosynthesis of tailored-made helical nanoswimmers, Nanoscale 6 (2014) 9415–9420.
[61] S. Meng, Y. Zhang, Y. Liu, Z. Zhang, K. Ma, X. Chen, Q. Gao, X. Ma, W. Wang, H. Feng, The effect of particle size on the dynamics of self-electrophoretic Janus micromotors, sputtering distribution, and rectifying voltage, JCIS Open 5 (2022), 100046.
[62] T.S. Skelhon, Y. Chen, S.A.F. Bon, Hierarchical self-assembly of 'hard–soft' Janus particles into colloidal molecules and larger supracolloidal structures, Soft Matter 10 (2014) 7730–7735.
[63] W. Wang, W. Duan, A. Sen, T.E. Mallouk, Catalytically powered dynamic assembly of rod-shaped nanomotors and passive tracer particles, Proc. Natl. Acad. Sci. U. S. A. 110 (2013) 17744–17749.
[64] Y. Mei, G. Huang, A.A. Solovev, E.B. Ureña, I. Mönch, F. Ding, T. Reindl, R.K. Y. Fu, P.K. Chu, O.G. Schmidt, Versatile approach for integrative and functionalized tubes by strain engineering of nanomembranes on polymers, Adv. Mater. 20 (2008) 4085–4090.
[65] A.A. Solovev, Y. Mei, E. Bermúdez Ureña, G. Huang, O.G. Schmidt, Catalytic microtubular jet engines self-propelled by accumulated gas bubbles, Small 5 (2009) 1688–1692.
[66] G. Zhao, A. Ambrosi, M. Pumera, Clean room-free rapid fabrication of roll-up self-powered catalytic microengines, J. Mater. Chem. A 2 (2013) 1219–1223.
[67] Y. Wu, Z. Wu, X. Lin, Q. He, J. Li, Autonomous movement of controllable assembled janus capsule motors, ACS Nano 6 (2012) 10910–10916.
[68] Z. Wu, Y. Wu, W. He, X. Lin, J. Sun, Q. He, Self-propelled polymer-based multilayer nanorockets for transportation and drug release, Angew. Chem. Int. Ed. 52 (2013) 7000–7003.
[69] M. Urso, M. Ussia, M. Pumera, Smart micro- and nanorobots for water purification, Nat Rev Bioeng 1 (2023) 236–251.
[70] A.C. Hortelao, C. Simó, M. Guix, S. Guallar-Garrido, E. Julián, D. Vilela, L. Rejc, P. Ramos-Cabrer, U. Cossío, V. Gómez-Vallejo, et al., Swarming behavior and in vivo monitoring of enzymatic nanomotors within the bladder, Sci. Robot. 6 (2021), eabd2823.
[71] V. Magdanz, S. Sanchez, O.G. Schmidt, Development of a sperm-flagella driven micro-bio-robot, Adv. Mater. 25 (2013) 6581–6588.
[72] S. Keller, S.P. Teora, G.X. Hu, M. Nijemeisland, D.A. Wilson, High-throughput design of biocompatible enzyme-based hydrogel microparticles with autonomous movement, Angew. Chem. Int. Ed. 57 (2018) 9814–9817.
[73] M. Zou, J. Wang, Y. Yu, L. Sun, H. Wang, H. Xu, Y. Zhao, Composite multifunctional micromotors from droplet microfluidics, ACS Appl. Mater. Interfaces 10 (2018) 34618–34624.
[74] M.-J. Tang, W. Wang, Z.-L. Li, Z.-M. Liu, Z.-Y. Guo, H.-Y. Tian, Z. Liu, X.-J. Ju, R. Xie, L.-Y. Chu, Controllable microfluidic fabrication of magnetic hybrid microswimmers with hollow helical structures, Ind. Eng. Chem. Res. 57 (2018) 9430–9438.
[75] X. Du, Q. Li, G. Wu, S. Chen, Multifunctional micro/nanoscale fibers based on microfluidic spinning technology, Adv. Mater. 31 (2019), 1903733.
[76] F. Qin, Y. Zhang, F. Peng, Fabrication of magnetically driven helical micro/nanoscale motors and their functionalization for targeted drug delivery, ChemNanoMat 7 (2021) 415–428.
[77] M. Ren, W. Guo, H. Guo, X. Ren, Microfluidic fabrication of bubble-propelled micromotors for wastewater treatment, ACS Appl. Mater. Interfaces 11 (2019) 22761–22767.
[78] K.D. Seo, B.K. Kwak, S. Sanchez, D.S. Kim, Microfluidic-assisted fabrication of flexible and location traceable organo-motor, IEEE Trans. Nanobioscience 14 (2015) 298–304.

[79] Y. Yu, L. Shang, W. Gao, Z. Zhao, H. Wang, Y. Zhao, Microfluidic lithography of bioinspired helical micromotors, Angew. Chem. Int. Ed. 56 (2017) 12127–12131.
[80] H. Duan, M. Huo, Y. Fan, From animal collective behaviors to swarm robotic cooperation, Natl. Sci. Rev. 10 (2023), nwad040.
[81] L. Yang, J. Jiang, X. Gao, Q. Wang, Q. Dou, L. Zhang, Autonomous environment-adaptive microrobot swarm navigation enabled by deep learning-based real-time distribution planning, Nat. Mach. Intell. 4 (2022) 480–493.
[82] S. Sengupta, K.K. Dey, H.S. Muddana, T. Tabouillot, M.E. Ibele, P.J. Butler, A. Sen, Enzyme molecules as nanomotors, J. Am. Chem. Soc. 135 (2013) 1406–1414.
[83] Y. Sun, R. Pan, Y. Chen, Y. Wang, L. Sun, N. Wang, X. Ma, G.P. Wang, Efficient preparation of a magnetic helical carbon nanomotor for targeted anticancer drug delivery, ACS Nanosci. Au 3 (2023) 94–102.
[84] M. Liu, L. Chen, Z. Zhao, M. Liu, T. Zhao, Y. Ma, Q. Zhou, Y.S. Ibrahim, A. A. Elzatahry, X. Li, et al., Enzyme-based mesoporous nanomotors with near-infrared optical brakes, J. Am. Chem. Soc. 144 (2022) 3892–3901.
[85] J. Guo, J.J. Gallegos, A.R. Tom, D. Fan, Electric-field-guided precision manipulation of catalytic nanomotors for cargo delivery and powering nanoelectromechanical devices, ACS Nano 12 (2018) 1179–1187.
[86] P. Calvo-Marzal, K.M. Manesh, D. Kagan, S. Balasubramanian, M. Cardona, G.-U. Flechsig, J. Posner, J. Wang, Electrochemically-triggered motion of catalytic nanomotors, Chem. Commun. (2009) 4509.
[87] J. Wang, X. Liu, Y. Qi, Z. Liu, Y. Cai, R. Dong, Ultrasound-propelled nanomotors for improving antigens cross-presentation and cellular immunity, Chem. Eng. J. 416 (2021), 129091.
[88] Z. Lin, C. Gao, M. Chen, X. Lin, Q. He, Collective motion and dynamic self-assembly of colloid motors, Curr. Opin. Colloid Interface Science 35 (2018) 51–58.
[89] Q. Wang, L. Zhang, External power-driven microrobotic swarm: from fundamental understanding to imaging-guided delivery, ACS Nano 15 (2021) 149–174.
[90] H. Xie, M. Sun, X. Fan, Z. Lin, W. Chen, L. Wang, L. Dong, Q. He, Reconfigurable magnetic microrobot swarm: multimode transformation, locomotion, and manipulation, Sci. Robot. 4 (2019), eaav8006.
[91] B. Dai, J. Wang, Z. Xiong, X. Zhan, W. Dai, C.-C. Li, S.-P. Feng, J. Tang, Programmable artificial phototactic microswimmer, Nat. Nanotechnol. 11 (2016) 1087–1092.
[92] C. Wu, J. Dai, X. Li, L. Gao, J. Wang, J. Liu, J. Zheng, X. Zhan, J. Chen, X. Cheng, et al., Ion-exchange enabled synthetic swarm, Nat. Nanotechnol. 16 (2021) 288–295.
[93] Z. Li, H. Zhang, D. Wang, C. Gao, M. Sun, Z. Wu, Q. He, Reconfigurable assembly of active liquid metal colloidal cluster, Angew. Chem. Int. Ed. 59 (2020) 19884–19888.
[94] S. Tang, F. Zhang, J. Zhao, W. Talaat, F. Soto, E. Karshalev, C. Chen, Z. Hu, X. Lu, J. Li, et al., Structure-dependent optical modulation of propulsion and collective behavior of acoustic/light-driven hybrid microbowls, Adv. Funct. Mater. 29 (2019), 1809003.
[95] Y. Gao, Z. Xiong, J. Wang, J. Tang, D. Li, Light hybrid micro/nano-robots: from propulsion to functional signals, Nano Res 15 (2022) 5355–5375.
[96] A. Bricard, J.-B. Caussin, N. Desreumaux, O. Dauchot, D. Bartolo, Emergence of macroscopic directed motion in populations of motile colloids, Nature 503 (2013) 95–98.
[97] A. Somasundar, S. Ghosh, F. Mohajerani, L.N. Massenburg, T. Yang, P.S. Cremer, D. Velegol, A. Sen, Positive and negative chemotaxis of enzyme-coated liposome motors, Nat. Nanotechnol. 14 (2019) 1129–1134.
[98] X. Zhao, A. Sen, Metabolon formation by chemotaxis. Methods in Enzymology, Elsevier, 2019, pp. 45–62.
[99] F. Ji, Y. Wu, M. Pumera, L. Zhang, Collective behaviors of active matter learning from natural taxes across scales, Adv. Mater. 35 (2023), 2203959.
[100] J. Parmar, D. Vilela, K. Villa, J. Wang, S. Sánchez, Micro- and nanomotors as active environmental microcleaners and sensors, J. Am. Chem. Soc. 140 (2018) 9317–9331.
[101] Y. Zhang, K. Yan, F. Ji, L. Zhang, Enhanced removal of toxic heavy metals using swarming biohybrid adsorbents, Adv. Funct. Mater. 28 (2018), 1806340.
[102] M. Sun, W. Chen, X. Fan, C. Tian, L. Sun, H. Xie, Cooperative recyclable magnetic microsubmarines for oil and microplastics removal from water, Appl. Mater. Today 20 (2020), 100682.
[103] L. Wang, A. Kaeppler, D. Fischer, J. Simmchen, Photocatalytic TiO_2 micromotors for removal of microplastics and suspended matter, ACS Appl. Mater. Interfaces 11 (2019) 32937–32944.
[104] H. Park, A. May, L. Portilla, H. Dietrich, F. Münch, T. Rejek, M. Sarcletti, L. Banspach, D. Zahn, M. Halik, Magnetite nanoparticles as efficient materials for removal of glyphosate from water, Nat. Sustain. 3 (2019) 129–135.
[105] Y. Hu, W. Liu, Y. Sun, Multiwavelength phototactic micromotor with controllable swarming motion for "Chemistry-on-the-Fly", ACS Appl. Mater. Interfaces 12 (2020) 41495–41505.
[106] J. Law, X. Wang, M. Luo, L. Xin, X. Du, W. Dou, T. Wang, G. Shan, Y. Wang, P. Song, et al., Microrobotic swarms for selective embolization, Sci. Adv. 8 (2022), eabm5752.
[107] M. Sun, K.F. Chan, Z. Zhang, L. Wang, Q. Wang, S. Yang, S.M. Chan, P.W.Y. Chiu, J.J.Y. Sung, L. Zhang, Magnetic microswarm and fluoroscopy-guided platform for biofilm eradication in biliary stents, Adv. Mater. 34 (2022), 2201888.
[108] M. Hoop, Y. Shen, X.-Z. Chen, F. Mushtaq, L.M. Iuliano, M.S. Sakar, A. Petruska, M.J. Loessner, B.J. Nelson, S. Pané, Magnetically driven silver-coated nanocoils for efficient bacterial contact killing, Adv. Funct. Mater. 26 (2016) 1063–1069.
[109] Q. Wang, B. Wang, J. Yu, K. Schweizer, B.J. Nelson, L. Zhang, Reconfigurable magnetic microswarm for thrombolysis under ultrasound imaging. 2020 IEEE International Conference on Robotics and Automation ((ICRA)), IEEE,, 2020, pp. 10285–10291.
[110] H. Zhang, Z. Li, C. Gao, X. Fan, Y. Pang, T. Li, Z. Wu, H. Xie, Q. He, Dual-responsive biohybrid neutrobots for active target delivery, Sci. Robot. 6 (2021), eaaz9519.
[111] I.B. Nava-Medina, K.A. Gold, S.M. Cooper, K. Robinson, A. Jain, Z. Cheng, A. K. Gaharwar, Self-oscillating 3D printed hydrogel shapes, Adv. Mater. Technol. 6 (2021), 2100418, https://doi.org/10.1002/admt.202100418.
[112] K. Inui, T. Watanabe, H. Minato, S. Matsui, K. Ishikawa, R. Yoshida, D. Suzuki, The Belousov–Zhabotinsky reaction in thermoresponsive core–shell hydrogel microspheres with a Tris(2,2′-bipyridyl)ruthenium catalyst in the core, J. Phys. Chem. B 124 (2020) 3828–3835.
[113] R. Yoshida, 9 - Self-oscillating polymer gels as novel biomimetic materials, in: T. D. Ngo (Ed.), Biomimetic Technologies Woodhead Publishing Series in Electronic and Optical Materials., Woodhead Publishing, 2015, pp. 181–198.
[114] R. Teng, L. Ren, L. Yuan, L. Wang, Q. Gao, I.R. Epstein, Effect of reaction parameters on the wavelength of pulse waves in the belousov–zhabotinsky reaction–diffusion system, J. Phys. Chem. A 123 (2019) 9292–9297.
[115] N.J. Suematsu, Y. Mori, T. Amemiya, S. Nakata, Oscillation of speed of a self-propelled Belousov–Zhabotinsky droplet, J. Phys. Chem. Lett. 7 (2016) 3424–3428.
[116] T. Geher-Herczegh, Z. Wang, T. Masuda, R. Yoshida, N. Vasudevan, Y. Hayashi, Delayed mechanical response to chemical kinetics in self-oscillating hydrogels driven by the Belousov–Zhabotinsky reaction, Macromolecules 54 (2021) 6430–6439.
[117] S. Maeda, Y. Hara, T. Sakai, R. Yoshida, S. Hashimoto, Self-walking gel, Adv. Mater. 19 (2007) 3480–3484.
[118] S.G.J. Postma, I.N. Vialshin, C.Y. Gerritsen, M. Bao, W.T.S. Huck, Preprogramming complex hydrogel responses using enzymatic reaction networks, Angew. Chem. Int. Ed. 56 (2017) 1794–1798.
[119] S.N. Semenov, L.J. Kraft, A. Ainla, M. Zhao, M. Baghbanzadeh, V.E. Campbell, K. Kang, J.M. Fox, G.M. Whitesides, Autocatalytic, bistable, oscillatory networks of biologically relevant organic reactions, Nature 537 (2016) 656–660.
[120] S. Matsui, K. Inui, Y. Kumai, R. Yoshida, D. Suzuki, Autonomously oscillating hydrogel microspheres with high-frequency swelling/deswelling and dispersing/flocculating oscillations, ACS Biomater. Sci. Eng. 5 (2019) 5615–5622.
[121] H. Jahangirian, K. Kalantari, Z. Izadiyan, R. Rafiee-Moghaddam, K. Shameli, T. J. Webster, A review of small molecules and drug delivery applications using gold and iron nanoparticles, IJN Volume 14 (2019) 1633–1657.
[122] A. Pugazhendhi, T.N.J.I. Edison, I. Karuppusamy, B. Kathirvel, Inorganic nanoparticles: a potential cancer therapy for human welfare, Inter. J. Pharm. 539 (2018) 104–111.
[123] S. Hong, D.W. Choi, H.N. Kim, C.G. Park, W. Lee, H.H. Park, Protein-based nanoparticles as drug delivery systems, Pharmaceutics 12 (2020) 604.
[124] A.O. Elzoghby, W.M. Samy, N.A. Elgindy, Albumin-based nanoparticles as potential controlled release drug delivery systems, J. Control. Release 157 (2012) 168–182.
[125] F. Danhier, E. Ansorena, J.M. Silva, R. Coco, A. Le Breton, V. Préat, PLGA-based nanoparticles: an overview of biomedical applications, J. Control. Release 161 (2012) 505–522.
[126] Y. Ding, Z. Jiang, K. Saha, C.S. Kim, S.T. Kim, R.F. Landis, V.M. Rotello, Gold nanoparticles for nucleic acid delivery, Mol. Ther. 22 (2014) 1075–1083.
[127] S.S. Lucky, K.C. Soo, Y. Zhang, Nanoparticles in photodynamic therapy, Chem. Rev. 115 (2015) 1990–2042.
[128] D.A. Urban, L. Rodriguez-Lorenzo, S. Balog, C. Kinnear, B. Rothen-Rutishauser, A. Petri-Fink, Plasmonic nanoparticles and their characterization in physiological fluids, Colloids and Surf. B: Biointerfaces 137 (2016) 39–49.
[129] C. Kinnear, T.L. Moore, L. Rodriguez-Lorenzo, B. Rothen-Rutishauser, A. Petri-Fink, Form follows function: nanoparticle shape and its implications for nanomedicine, Chem. Rev. 117 (2017) 11476–11521.
[130] M.S. Almeida, de, E. Susnik, B. Drasler, P. Taladriz-Blanco, A. Petri-Fink, B. Rothen-Rutishauser, Understanding nanoparticle endocytosis to improve targeting strategies in nanomedicine, Chem. Soc. Rev. 50 (2021) 5397–5434.
[131] D. Burnand, A. Milosevic, S. Balog, M. Spuch-Calvar, B. Rothen-Rutishauser, J. Dengjel, C. Kinnear, T.L. Moore, A. Petri-Fink, Beyond global charge: role of amine bulkiness and protein fingerprint on nanoparticle–cell interaction, Small 14 (2018), 1802088.
[132] K. Fytianos, S. Chortarea, L. Rodriguez-Lorenzo, F. Blank, C. von Garnier, A. Petri-Fink, B. Rothen-Rutishauser, Aerosol delivery of functionalized gold nanoparticles target and activate dendritic cells in a 3D lung cellular model, ACS Nano 11 (2017) 375–383.
[133] C. Kinnear, L. Rodriguez-Lorenzo, M.J.D. Clift, B. Goris, S. Bals, B. Rothen-Rutishauser, A. Petri-Fink, Decoupling the shape parameter to assess gold nanorod uptake by mammalian cells, Nanoscale 8 (2016) 16416–16426.
[134] D. Septiadi, J. Bourquin, E. Durantie, A. Petri-Fink, B. Rothen-Rutishauser, A novel sample holder for 4D live cell imaging to study cellular dynamics in complex 3D tissue cultures, Sci. Rep. 8 (2018) 9861.
[135] S. Hočevar, V. Puddinu, L. Haeni, A. Petri-Fink, J. Wagner, M. Alvarez, M.J. D. Clift, C. Bourquin, PEGylated Gold Nanoparticles Target Age-associated B Cells In Vivo, ACS Nano 16 (2022) 18119–18132.
[136] D. Septiadi, F. Crippa, T.L. Moore, B. Rothen-Rutishauser, A. Petri-Fink, Nanoparticle–Cell Interaction: a Cell Mechanics Perspective, Adv. Mater. 30 (2018), 1704463.

[137] F. Crippa, B. Rothen-Rutishauser, A. Petri-Fink, Magneto-responsive Cell Culture Substrates That Can Be Modulated in situ, CHIMIA 73 (2019), 51–51.
[138] H.V. Nguyen, V. Faivre, Targeted drug delivery therapies inspired by natural taxes, J. Control. Release 322 (2020) 439–456.
[139] A. Reece, B. Xia, Z. Jiang, B. Noren, R. McBride, J. Oakey, Microfluidic techniques for high throughput single cell analysis, Curr. Opin. Biotechnol. 40 (2016) 90–96.
[140] T.S. Kaminski, O. Scheler, P. Garstecki, Droplet microfluidics for microbiology: techniques, applications and challenges, Lab Chip 16 (2016) 2168–2187.
[141] Y. Zhu, Q. Fang, Analytical detection techniques for droplet microfluidics—a review, Anal. Chim. Acta 787 (2013) 24–35.
[142] R.T. Kelly, Jin-Ming Lin (Ed.): cell analysis on microfluidics, Anal. Bioanal. Chem. 410 (2018) 7825–7826.
[143] H.N. Joensson, H. Andersson Svahn, Droplet microfluidics—a tool for single-cell analysis, Angew. Chem. Int. Ed. 51 (2012) 12176–12192.
[144] M. Moarefian, R.V. Davalos, D.K. Tafti, L.E. Achenie, C.N. Jones, Modeling iontophoretic drug delivery in a microfluidic device, Lab Chip 20 (2020) 3310–3321.
[145] J.J. Sherba, S. Hogquist, H. Lin, J.W. Shan, D.I. Shreiber, J.D. Zahn, The effects of electroporation buffer composition on cell viability and electro-transfection efficiency, Sci. Rep. 10 (2020) 3053.
[146] S. Movahed, D. Li, Microfluidics cell electroporation, Microfluid. Nanofluid 10 (2011) 703–734.
[147] S. Wang, L.J. Lee, Micro-/nanofluidics based cell electroporation, Biomicrofluidics 7 (2013), 011301.
[148] B. Qu, Y.-J. Eu, W.-J. Jeong, D.-P. Kim, Droplet electroporation in microfluidics for efficient cell transformation with or without cell wall removal, Lab Chip 12 (2012) 4483–4488.
[149] D.L. West, S.B. White, Z. Zhang, A.C. Larson, R.A. Omary, Assessment and optimization of electroporation-assisted tumoral nanoparticle uptake in a nude mouse model of pancreatic ductal adenocarcinoma, Int. J. Nanosci. 9 (2014) 4169–4176.
[150] S. van Drunen Littel-van den Hurk, D. Hannaman, Electroporation for DNA immunization: clinical application, Expert Rev. Vaccines 9 (2010) 503–517.
[151] C.A. Lissandrello, J.A. Santos, P. Hsi, M. Welch, V.L. Mott, E.S. Kim, J. Chesin, N. J. Haroutunian, A.G. Stoddard, A. Czarnecki, et al., High-throughput continuous-flow microfluidic electroporation of mRNA into primary human T cells for applications in cellular therapy manufacturing, Sci. Rep. 10 (2020) 18045.
[152] M. Khine, A. Lau, C. Ionescu-Zanetti, J. Seo, L.P. Lee, A single cell electroporation chip, Lab Chip 5 (2005) 38–43.